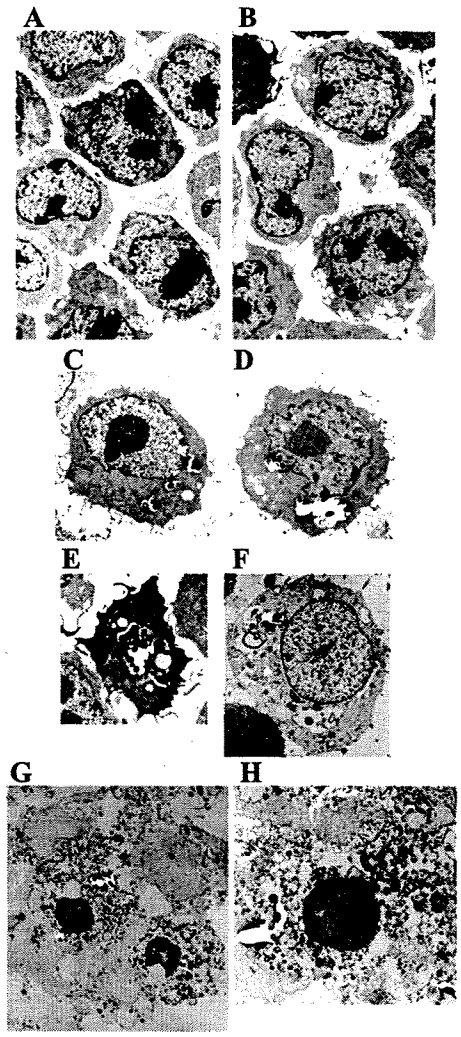

FIG. 3. Effect of z-VAD-fmk on morphologies of infected cells. RAW 264 cells infected with H37Rv were cultured for 3 days in the absence (C to F) or presence (G, H) of z-VAD-fmk. Cells were fixed, and morphologies were observed under an electron microscope. (E) A representative apoptotic cell. (F) A cell showing necrotic damage. (C and D) Infected cells which maintained normal cell morphologies. (A and B) Nontreated cells (A) and cells treated only with z-VAD-fmk (B). Micrographs were taken at magnifications of ×5,000 (A to F and H) and ×3,000 (G).

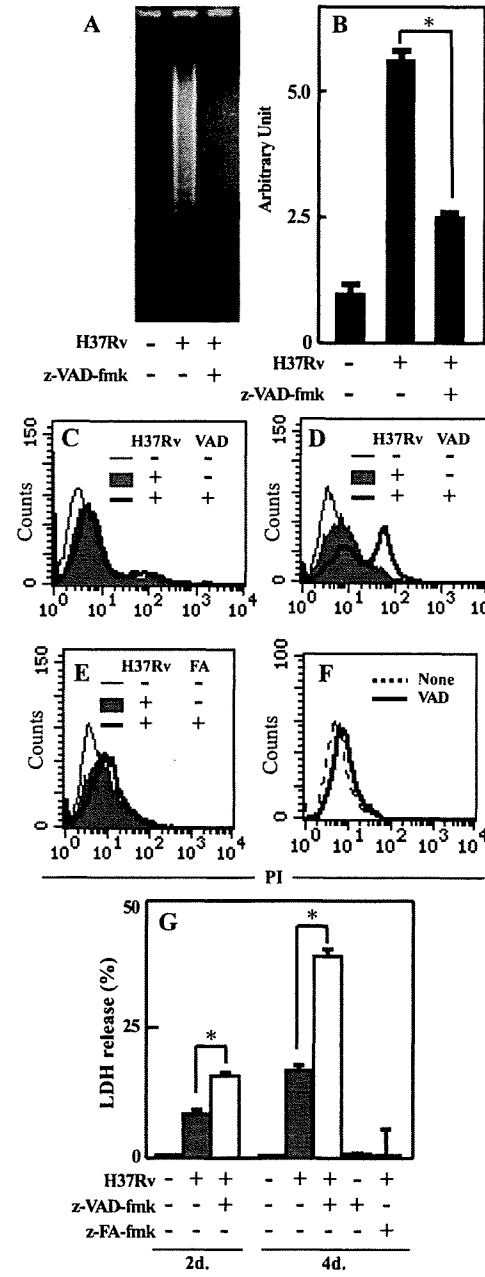

FIG. 4. Inhibition of apoptosis and induction of necrosis by z-VAD-fmk treatment. RAW 264 cells were infected with H37Rv and cultured for 2 days. Cells were lysed, and the DNA ladder and oligonucleosomes were detected by agarose gel electrophoresis (A) and quantified by an enzyme-linked immunosorbent assay (B), respectively. Two days (C) and 4 days (D, E) after infection, the cells were stained with PI and fluorescence intensity was measured. VAD, z-VAD-fmk; FA, z-FA-fmk. (F) Fluorescence intensity of the cells treated only with z-VAD-fmk for 4 days. (G) Culture supernatants were collected 2 and 4 days after infection, and LDH activity was assayed. Data represent the means ± standard deviations for triplicate assays and are representative of three independent experiments. *, $P < 0.05$.

much severe damage in the infected cells. As shown in Fig. 3G and H, the caspase inhibitor caused necrotic morphological changes in as many as 95% of the infected cells. These results raised the possibility that some caspases contribute to inhibition of necrosis of infected cells in conventional infection in vitro. To confirm that the morphological changes resulted from apoptosis or necrosis of the infected cells, we investigated a generation of oligonucleosomes and assessed the membrane integrity of the infected cells by measuring the population of PI-stained cells and LDH release into the culture medium. As shown in Fig. 4A, an oligonucleosomal DNA ladder was observed in RAW 264 cells infected with H37Rv but not in uninfected cells. Treatment with z-VAD-fmk clearly inhibited the cleavage of DNA. To analyze the DNA fragmentation quantitatively, the cell lysates were subjected to a sandwich enzyme-linked immunosorbent assay specific for oligonucleosomes. The number of oligonucleosomes in H37Rv-infected cells was about 5 times as high as that in the uninfected cells, but z-VAD-fmk significantly inhibited the generation of oligo-

nucleosomes (Fig. 4B). These results clearly indicated that z-VAD-fmk inhibited the apoptotic process induced by infection with H37Rv. On the other hand, though the infected cells were not stained with PI for 2 days after infection, irrespective of z-VAD-fmk treatment, the fluorescence intensities in both groups increased at day 4 postinfection (Fig. 4C and D). In the absence of z-VAD-fmk treatment, cells were stained intermediately with PI and could be divided into two populations based on fluorescence intensity. Since the number of cells expressing the brighter fluorescence reached 32.2% of the total number of cells and 32% of the infected cells exhibited necrotic morphologies (Fig. 3), it seemed that the cells stained highly with PI represented the cells undergoing necrosis. On the other hand, most of the z-VAD-fmk-treated cells were stained strongly with PI 4 days after infection, while z-FA-fmk treatment did not increase the number of damaged cells in the population (Fig. 4E). PI-stained cells were never observed in noninfected cells treated with z-VAD-fmk alone (Fig. 4F). In addition, z-VAD-fmk treatment caused a lower but a significant level of LDH release from the infected cells 2 days after infection, and the release was dramatically enhanced on day 4. Again, there was no LDH release at all from the cells treated with z-VAD-fmk alone even after 4 days in the absence of *M. tuberculosis* infection (Fig. 4G). Furthermore, z-FA-fmk treatment did not induce LDH release from the infected cells. These results strongly suggested that H37Rv induced the activation of caspases, resulting in not only the induction of apoptosis but also the inhibition of necrosis of infected cells.

Involvement of ROS accumulation in z-VAD-fmk-induced necrosis of infected cells. Vercammen et al. have shown that L929 fibrosarcoma cells treated with z-VAD-fmk rapidly died from necrosis after treatment with TNF-α. Necrotic cell death was induced also by overexpression of cytokine response modifier A (CrmA), a serpin-like caspase inhibitor (12, 32). In these reports, they indicated that the necrosis was provoked by ROS that was generated by inhibition of caspases. Since H37Rv infection induced severe necrosis of infected cells when the cells were treated with a caspase inhibitor, we examined whether z-VAD-fmk treatment triggers ROS generation in H37Rv-infected cells by using DCFH-DA, a fluorescent detector of ROS. RAW 264 cells were infected with H37Rv for 2 days in the presence or absence of z-VAD-fmk and treated with DCFH-DA for 15 min. The fluorescence of DCFH emitted in cytoplasm after oxidization by ROS was measured by FACSCalibur. The fluorescence intensity of the infected cells was increased significantly by treatment with z-VAD-fmk (Fig. 5A). However, enhancement of fluorescence was diminished by addition of BHA, a scavenger of ROS generated intracellularly, indicating that z-VAD-fmk treatment induced the generation of ROS in the infected cells (Fig. 5B). We further found that BHA treatment suppressed the z-VAD-fmk-induced necrosis of H37Rv-infected cells, because both the fluorescence intensity of the PI-stained cells and the LDH release from the cells were decreased markedly by BHA (Fig. 5C and D). In addition, though treatment with z-VAD-fmk inhibited the intracellular growth of H37Rv, the inhibitory activity was cancelled appreciably by treatment with BHA (Fig. 5E). Furthermore, our data showed that the low level of intracellular ROS that was generated by H37Rv alone did not affect the bacterial growth, because BHA treatment did not influence the

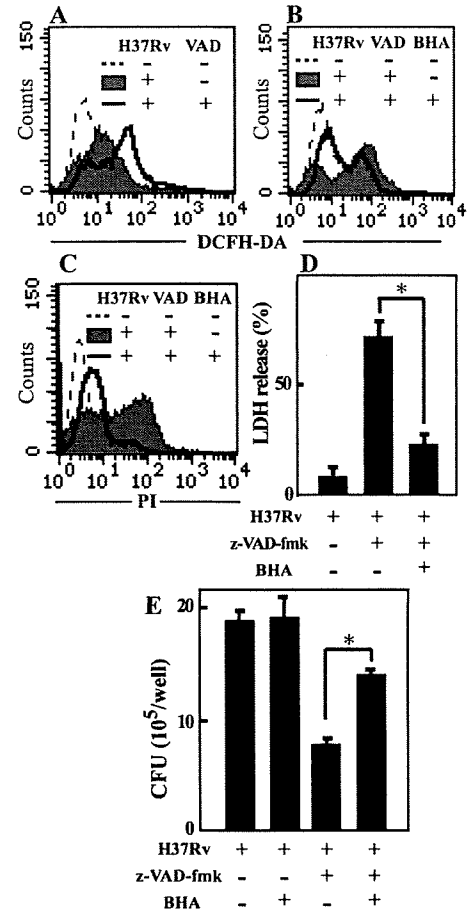

FIG. 5. Involvement of intracellular ROS accumulation in induction of necrosis and inhibition of intracellular bacterial growth. (A) RAW 264 cells were infected with H37Rv and cultured for 2 days in the presence or absence of z-VAD-fmk. Cells were treated with 5 μM DCFH-DA, and the fluorescence intensity of the oxidized DCFH was measured. (B) RAW 264 cells were infected and cultured for 2 days with or without z-VAD-fmk and an antioxidant reagent, BHA (25 μM). The cells were treated with DCFH-DA, and fluorescence intensity was measured. (C) Two days after infection, the cells were collected and cell permeability to PI was measured. (D) RAW 264 cells were infected and cultured for 4 days. The culture supernatant was collected, and the LDH activity was measured. (E) RAW 264 cells were infected and cultured for 7 days with or without z-VAD-fmk and BHA. The cells were lysed, and the number of intracellular bacteria was determined. Data represent the means ± standard deviations for triplicate assays and are representative of three independent experiments. *, $P < 0.05$.

intracellular bacterial number. These results indicated that inhibition of caspase activities by z-VAD-fmk induced the high level of ROS generation in the cytoplasm of H37Rv-infected cells. The intracellular ROS appeared to contribute to the induction of necrosis and the arrest of intracellular growth of H37Rv.

Critical involvement of caspase-9 in the inhibition of necrosis. Because z-VAD-fmk is a broad-spectrum caspase inhibitor capable of inhibiting the activity of caspases in general (23, 27), we next tried to identify the particular caspase involved in the inhibition of necrosis of infected cells. To address this point, we employed specific inhibitors for caspase-1, caspase-2,

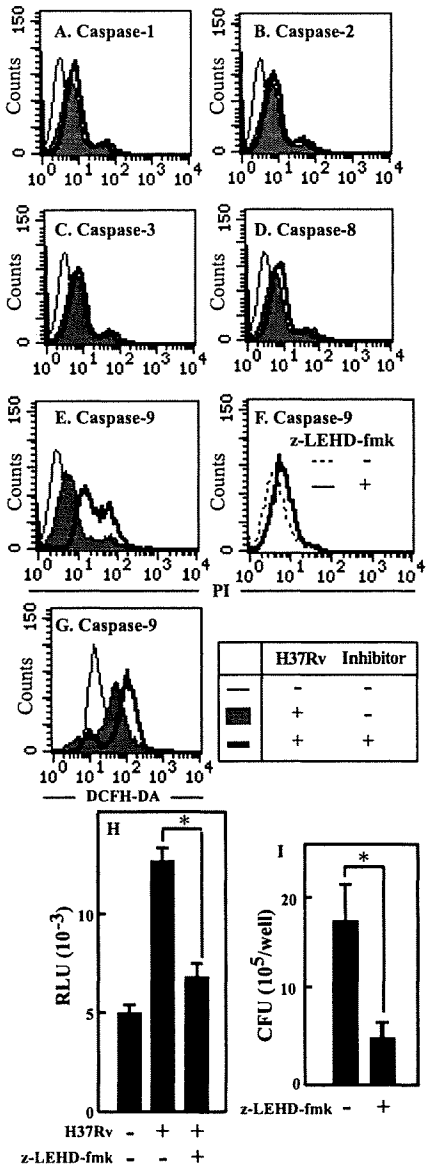

FIG. 6. Effects of inhibitors (120 μM) for caspase-1, -2, -3, -8, and -9 on induction of necrosis and intracellular bacterial growth. RAW 264 cells were infected with H37Rv and incubated with or without inhibitors specific for caspase-1 (A), caspase-2 (B), caspase-3 (C), caspase-8 (D), or caspase-9 (E). After 3 days of cultivation, membrane permeability was assessed by PI staining. (F) The caspase-9 inhibitor does not affect membrane permeability. (G) RAW 264 cells were infected and cultured for 2 days with or without z-LEHD-fmk, and the cells were stained with DCFH-DA and measured for fluorescence derived from oxidized DCFH. (H) RAW 264 cells were infected and cultured for 2 days with or without z-LEHD-fmk. Caspase-9 activity was measured by a Caspase-Glo assay. (I) Seven days after infection and cultivation with z-LEHD-fmk, the number of intracellular bacteria was determined by a CFU assay. Data represent the means ± standard deviations for triplicate assays and are representative of three independent experiments. *, $P < 0.05$. RLU, relative light units.

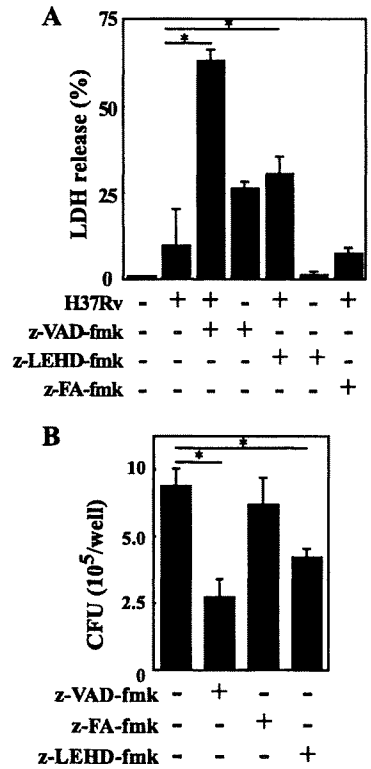

FIG. 7. Effects of caspase inhibitors on necrosis of H37Rv-infected macrophages and intracellular growth of bacteria. Peritoneal exudate macrophages were infected with H37Rv at an MOI of 5 in the presence or absence of caspase inhibitors. (A) Culture supernatants were collected 1 day after infection, and LDH activity was assayed. (B) Cells were infected with H37Rv and incubated for 7 days in the presence or absence of caspase inhibitors. The number of intracellular bacteria was determined by a CFU assay. Data represent the means ± standard deviations for triplicate assays and are representative of three independent experiments. *, $P < 0.05$.

caspase-3, caspase-8, and caspase-9 (10, 17, 31) instead of z-VAD-fmk and determined the effect of each inhibitor on necrosis of H37Rv-infected cells by measuring membrane permeability. Although inhibitors of caspase-1, caspase-2, caspase-3, and caspase-8 did not change the PI-staining pattern of the infected cells (Fig. 6A to D), only the caspase-9 inhibitor (z-LEHD-fmk) enhanced the fluorescence intensity (Fig. 6E). The inhibitor itself did not affect the membrane permeability (Fig. 6F). Furthermore, we found that z-LEHD-fmk enhanced the fluorescence intensity of oxidized DCFH in the infected cells (Fig. 6G) and inhibited the intracellular growth of H37Rv (Fig. 6I). Activation of caspase-9 in H37Rv-infected cells was significantly abolished in the presence of z-LEHD-fmk (Fig. 6H). These results suggested that caspase-9 which was activated by H37Rv infection contributed to the inhibition of necrosis through regulation of intracellular ROS generation.

Detection of caspase-9-dependent inhibition of bacterial growth and necrosis in peritoneal macrophages. To analyze whether caspase-9-dependent inhibition of necrosis is a general intracellular event after H37Rv infection, we infected thioglycolate-induced peritoneal macrophages with H37Rv in the presence or absence of z-VAD-fmk or z-LEHD-fmk and measured LDH release. Similar to H37Rv infection in RAW 264 cells, H37Rv induced only a low level of LDH release from the infected macrophages and z-FA-fmk did not augment the response (Fig. 7A). However, treatment with z-VAD-fmk and z-LEHD-fmk caused a high level of LDH release from the infected macrophages compared to treatment with caspase

inhibitor alone or H37Rv infection without treatment with these inhibitors (Fig. 7A). In addition, we found that treatment with z-VAD-fmk or z-LEHD-fmk significantly reduced the intracellular number of bacteria (Fig. 7B). These data are consistent with those obtained from RAW 264 cells, suggesting that caspase-9 generally contributes to inhibition of necrosis in macrophages after *M. tuberculosis* infection.

Difference between the abilities of H37Rv and H37Ra to induce necrosis and apoptosis and activate caspase-9. We next investigated the abilities of H37Rv and H37Ra in induction of apoptosis and necrosis and activation of caspase in RAW 264 cells to determine whether H37Rv-induced responses are associated with the virulence of *M. tuberculosis*. Two days after infection, H37Rv induced LDH release from the infected cells while such a level of LDH release was not detected in the supernatant of cells infected with H37Ra (Fig. 8A). In contrast, a significant number of oligonucleosomes was detected in the lysate of H37Ra-infected cells, which was higher than that in the H37Rv-infected cells (Fig. 8B). In addition, we found that H37Ra induced a higher level of caspase-3/7 and caspase-8 activation than H37Rv. These results indicated that H37Rv but not H37Ra caused necrosis of RAW 264 cells and that H37Ra had a higher ability in induction of apoptosis than H37Rv. In this experimental model, as described formerly, H37Rv induced a high level of LDH release from the cells cultured in the presence of z-VAD-fmk, while H37Ra caused only a moderate level of LDH release (Fig. 8A). In contrast to the strong activities of caspase-9 and the active caspase-9 fragment in the lysate of H37Rv-infected cells (Fig. 8C and D), H37Ra could not induce such levels of caspase-9 activation. The amount of the active form of caspase-9 detected in H37Ra infection was smaller than that induced by H37Rv infection (Fig. 8C and D). It may be suggested that virulent *M. tuberculosis* has the ability to cause necrosis of the infected macrophages but, at the same time, is capable of activating caspase-9 in order to evade immediate necrotic cell death after infection in host cells where *M. tuberculosis* must reside for a longer period.

DISCUSSION

In the present study, we showed that H37Rv induced the activation of various caspases and that some of the infected cells underwent apoptosis 2 days after infection. Our initial presumption was, therefore, that the addition of the broad-spectrum caspase inhibitor z-VAD-fmk might simply block the apoptosis of RAW 264 cells infected with H37Rv and facilitate the bacterial growth inside. Indeed, generation of oligonucleosomes, which is a representative parameter for apoptosis, was significantly inhibited by the addition of z-VAD-fmk. To our surprise, however, the treatment instead caused necrosis in a very high proportion of the infected cells. These results strongly suggested that some caspases contribute to the inhibition of necrosis of RAW 264 cells induced by H37Rv infection. By using a panel of inhibitors specific for each caspase, we were able to find that caspase-9 is responsible for such an effect through inhibition of intracellular ROS generation. The less virulent strain H37Ra hardly induced caspase-9 activation, and necrosis of infected cells could not be observed even in the presence of z-VAD-fmk. It was suggested that caspase-9-de-

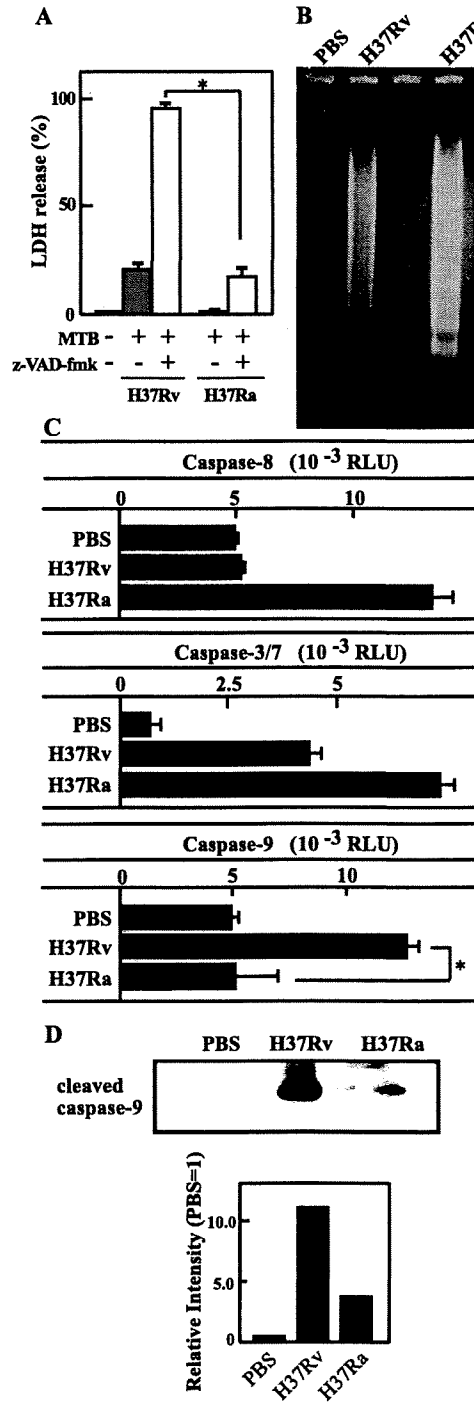

FIG. 8. Differences between the abilities of the *M. tuberculosis* H37Rv and H37Ra strains to induce apoptosis, necrosis, and caspase activation in RAW 264 cells. RAW 264 cells were infected with H37Rv or H37Ra at an MOI of 5 in the presence or absence of z-VAD-fmk. (A) The culture supernatant was collected 4 days later, and LDH activity was measured. Two days after cultivation, cells were lysed and the DNA ladder was detected by agarose gel electrophoresis (B) and caspase activities were measured by a Caspase-Glo assay (C). (D) The cell lysate was applied on a sodium dodecyl sulfate-polyacrylamide gel electrophoresis gel, and the amount of active form of caspase-9 was analyzed by Western blotting with caspase-9-specific antibody. The relative intensities of the bands are indicated in the lower graph. Data represent the means ± standard deviations for triplicate assays and are representative of three independent experiments. *, $P < 0.05$.

pendent inhibition of necrosis is related to the virulence of *M. tuberculosis*.

Based on our preliminary study, we selected concentrations of caspase inhibitors suitable for suppression of caspase activities. Schaible et al. used the caspase inhibitor z-VAD-fmk at the same concentration for their investigation (25). Although the appropriate concentration might be high, it might not be high, and it probably differs on the basis of experimental conditions. In the presence of a broad-spectrum caspase inhibitor or caspase-9-specific inhibitor, the growth of H37Rv was limited in RAW 264 cells that underwent necrosis. The current consensus is that apoptosis of macrophages results in the limitation of intracellular survival of *M. tuberculosis* but that necrosis does not affect the intracellular bacteria and helps *M. tuberculosis* in dissemination to other macrophages. Recent evidence further demonstrates that virulent *M. tuberculosis* possesses some inhibitory mechanisms of apoptosis that can be easily induced by less virulent strains (6, 15). In the present experiments, using RAW 264 cells, we observed that H37Ra induced a higher level of DNA fragmentation than H37Rv. In contrast, H37Rv infection caused a significant level of LDH release whereas H37Ra hardly induced LDH release during the initial period of infection. These results are consistent with observations published elsewhere (6, 15). In addition, we found that intracellular growth was inhibited in RAW 264 cells in which severe apoptosis was induced by treatment with actinomycin D (data not shown). As shown here, z-VAD-fmk and z-LEHD-fmk treatment caused severe necrosis of infected cells and the magnitude of necrosis was markedly different from that induced by H37Rv infection alone. It appears that induction of an excessive level of necrosis or apoptosis may eliminate the favorable niche for bacterial growth, resulting in the inhibition of bacterial multiplication in host cells. Our finding is not against the consensus, and we believe that this study could give insight into the role of caspase-9 in the fate of intracellular *M. tuberculosis*. Although the present data did not reveal whether necrosis of the infected macrophages affected bacterial replication in vivo, it has been reported that uncontrolled mycobacterial growth was observed in necrotic regions in the lungs of *sst1*^{s} mice and TNF-α or gamma interferon knockout mice (4, 8, 11, 19, 24). Because activation of the necrosis pathway may allow acceleration of bacterial growth and exacerbation of mycobacterial infection, the caspase-9-dependent necrosis inhibition that was presented in this study may be of additional importance in host defense against infection with virulent *M. tuberculosis*.

It has been shown that several kinds of caspase species contribute to inhibition of necrosis (18). Vercammen et al. have reported that TNF-α-stimulated L929 cells undergo necrosis when the cells are treated with a caspase inhibitor. They suggested that caspase-1 and caspase-3 might play a role in the inhibition of both ROS generation and necrosis (12, 31). On the other hand, other reports have shown that interaction of FasL and Fas induces necrosis if caspase-8 is inhibited (13, 17, 31). It is reported that caspase-8 inhibits necrosis by inhibition of binding of receptor-interacting protein to the death domain of the Fas receptor (13). In the present study, using *M. tuberculosis* infection in vitro, we found that caspase-9, but not caspase-1, -3, or -8, exerted a critical role in the inhibition of necrosis. Since there were differences in the requirements of particular caspases to inhibit necrosis of infected cells, it appeared that distinctive signal pathways were activated. One possible interpretation for the caspase-9-dependent inhibition of necrosis is that caspase-9 contributes to stabilization of the mitochondrial membrane and inhibition of ROS production from mitochondria. It has been shown that an excessive generation of ROS was induced from mitochondria in L929 cells after stimulation with TNF-α in the presence of an inhibitor for caspase-1 or caspase-3 (12, 31). Matsumura et al. have shown that a reduction of mitochondrial transmembrane potential ($\Delta\psi m$) was observed in JmF cells treated with FasL and z-VAD-fmk (17) and that pyrrolidine dithiocarbamate, a metallo chelator and antioxidant, efficiently inhibited FasL-induced necrosis. Our preliminary study also showed that z-VAD-fmk treatment caused a reduction of $\Delta\psi m$ in H37Rv-infected cells (data not shown). Since the intracellular concentration of ROS was increased when cells were infected with H37Rv in the presence of the caspase-9 inhibitor, caspase-9 might contribute to the inhibition of mitochondrial membrane damage. Further studies are needed to determine the precise mechanism.

It has been reported that various bacterial components are involved in apoptosis induction in cells infected with *M. tuberculosis*. There are several reports showing that 19-kDa lipoprotein and lipomannan derived from *M. tuberculosis* induced the apoptosis of macrophages or neutrophils (1, 5, 6, 9, 16). It was also reported that TNF-α was produced after infection with *M. tuberculosis* and caused apoptosis of macrophages (2, 22). On the other hand, other reports demonstrated that *M. tuberculosis* possesses an activity inhibiting apoptosis induction. Sly et al. showed that H37Rv had a weaker activity in induction of apoptosis than the attenuated H37Ra strain, and this was due to up-regulation of antiapoptotic gene expression in H37Rv-infected cells (28). Because the intracellular growth of H37Ra in RAW 264 cells was limited compared to that of H37Rv (data not shown), it is possible that activation of the inhibitory process facilitates the intracellular replication of H37Rv. On the other hand, H37Rv caused necrosis when infected cells were treated with the caspase-9 inhibitor. However, H37Ra hardly induced necrosis of cells treated with the inhibitor. Furthermore, we found that caspase-9 was not activated by infection with the attenuated H37Ra strain. Hsu et al. have shown that a mutant strain of H37Rv which is deficient for the *RD1* (region of difference 1) region is attenuated for virulence and necrosis-inducing abilities (14). In addition, Park et al. have shown that virulent clinical isolates of mycobacteria strongly induced necrosis of infected macrophages (20). Taken together, these results and our findings suggest that necrosis-inducing activity is associated with the virulence of *M. tuberculosis* and that caspase-9 activation is probably linked with some mycobacterial virulence determinant.

In conclusion, our present study clearly demonstrated that caspase-9 has a pivotal role in regulation of necrosis induced by infection with H37Rv. We are now trying to address how caspase-9 is activated and how the caspase inhibits necrosis of infected cells. In addition, because necrosis induction appears to be associated with the virulence of mycobacteria, further analysis on the bacterial factor responsible for caspase-9 induction may provide some novel insight for further understanding of host-*M. tuberculosis* interaction.

ACKNOWLEDGMENTS

This work was supported by a Grant-in-Aid for Scientific Research on Priority Areas (C) from the Ministry of Education, Science, Culture and Sports of Japan; by a Grant-in-Aid for Scientific Research (B and C) from The Japan Society for the Promotion of Science; and in part by a Grant-in-Aid for Scientific Research from the Ministry of Health, Labor and Welfare, Japan.

REFERENCES

1. **Alemán, M., P. Schierloh, S. S. de la Barrera, R. M. Musella, M. A Saab, M. Baldini, E. Abbate, and M. C. Sasiain.** 2004. *Mycobacterium tuberculosis* triggers apoptosis in peripheral neutrophils involving Toll-like receptor 2 and p38 mitogen protein kinase in tuberculosis patients. Infect. Immun. **72:**5150–5158.
2. **Balcewicz-Sablinska, M. K., J. Keane, H. Kornfeld, and H. G. Remold.** 1998. Pathogenic *Mycobacterium tuberculosis* evades apoptosis of host macrophages by release of TNF-R2, resulting in inactivation of TNF-α. J. Immunol. **161:**2636–2641.
3. **Bass, D. A., J. W. Parce, L. R. Dechatelet, P. Szejda, M. C. Seeds, and M. Thomas.** 1983. Flow cytometric studies of oxidative product formation by neutrophils: a graded response to membrane stimulation. J. Immunol. **130:**1910–1917.
4. **Bean, A. G. D., D. R. Roach, H. Briscoe, M. P. France, H. Korner, J. D. Sedgwick, and W. J. Britton.** 1999. Structural deficiencies in granuloma formation in TNF gene-targeted mice underlie the heightened susceptibility to aerosol *Mycobacterium tuberculosis* infection, which is not compensated for by lymphotoxin. J. Immunol. **162:**3504–3511.
5. **Ciaramella, A., A. Cavone, M. B. Santucci, S. K. Garg, N. Sanarico, M. Bocchino, D. Galati, A. Martino, G. Auricchio, M. D'Orazio, G. R. Stewart, O. Neyrolles, D. B. Young, V. Colizzi, and M. Fraziano.** 2004. Induction of apoptosis and release of interleukin-1β by cell wall-associated 19-kDa lipoprotein during the course of mycobacterial infection. J. Infect. Dis. **190:**1167–1176.
6. **Ciaramella, A., A. Martino, R. Cicconi, V. Colizzi, and M. Fraziano.** 2000. Mycobacterial 19-kDa lipoprotein mediates *Mycobacterium tuberculosis*-induced apoptosis in monocytes/macrophages at early stages of infection. Cell Death Differ. **7:**1270–1272.
7. **Clark-Curtiss, J. E., and S. E. Haydel.** 2003. Molecular genetics of *Mycobacterium tuberculosis* pathogenesis. Annu. Rev. Microbiol. **57:**517–549.
8. **Cooper, A. M., D. K. Dalton, T. A. Stewart, J. P. Griffin, D. G. Russell, and I. M. Orme.** 1993. Disseminated tuberculosis in interferon γ gene-disrupted mice. J. Exp. Med. **178:**2243–2247.
9. **Dao, D. N., L. Kremer, Y. Guérardel, A. Molano, W. R. Jacobs, Jr., S. A. Porcelli, and V. Briken.** 2004. *Mycobacterium tuberculosis* lipomannan induces apoptosis and interleukin-12 production in macrophages. Infect. Immun. **72:**2067–2074.
10. **Faraco, P. R., E. C. Ledgerwood, P. Vandenabeele, J. B. Prins, and J. R. Bradley.** 1999. Tumor necrosis factor induces distinct patterns of caspase activation in WEHI-164 cells associated with apoptosis or necrosis depending on cell cycle stage. Biochem. Biophys. Res. Commun. **261:**385–392.
11. **Flynn, J. L., J. Chan, K. J. Triebold, D. K. Dalton, T. A. Stewart, and B. R. Bloom.** 1993. An essential role for interferon γ in resistance to *Mycobacterium tuberculosis* infection. J. Exp. Med. **178:**2249–2254.
12. **Goossens, V., J. Grooten, K. de Vos, and W. Fiers.** 1995. Direct evidence for tumor necrosis factor-induced mitochondrial reactive oxygen intermediates and their involvement in cytotoxicity. Proc. Natl. Acad. Sci. USA **92:**8115–8119.
13. **Holler, N., R. Zaru, O. Micheau, M. Thome, A. Attinger, S. Valitutti, J.-L. Bodmer, P. Schneider, B. Seed, and J. Tschopp.** 2000. Fas triggers an alternative, caspase-8-independent cell death pathway using the kinase RIP as effector molecule. Nat. Immunol. **1:**489–495.
14. **Hsu, T., S. M. Hingley-Wilson, B. Chen, M. Chen, A. Z. Dai, P. M. Morin, C. B. Marks, J. Padiyar, C. Goulding, M. Gingery, D. Eisenberg, R. G. Russell, S. C. Derrick, F. M. Collins, S. L. Morris, C. H. King, and W. R. Jacobs, Jr.** 2003. The primary mechanism of attenuation of bacillus Calmette-Guérin is a loss of secreted lytic function required for invasion of lung interstitial tissue. Proc. Natl. Acad. Sci. USA **100:**12420–12425.
15. **Koul, A., T. Herget, B. Klebl, and A. Ullrich.** 2004. Interplay between mycobacteria and host signalling pathways. Nat. Rev. Microbiol. **2:**189–202.
16. **López, M., L. M. Sly, Y. Luu, D. Young, H. Cooper, and N. E. Reiner.** 2003. The 19-kDa *Mycobacterium tuberculosis* protein induces macrophage apoptosis through Toll-like receptor-2. J. Immunol. **170:**2409–2416.
17. **Matsumura, H., Y. Shimizu, Y. Ohsawa, A. Kawahara, Y. Uchiyama, and S. Nagata.** 2000. Necrotic death pathway in Fas receptor signaling. J. Cell Biol. **151:**1247–1255.
18. **Nicotera, P., and G. Melino.** 2004. Regulation of the apoptosis-necrosis switch. Oncogene **23:**2757–2765.
19. **Olleros, M. L., R. Guler, D. Vesin, R. Parapanov, G. Marchal, E. Martinez-Soria, N. Corazza, J.-C. Pache, C. Mueller, and I. Garcia.** 2005. Contribution of transmembrane tumor necrosis factor to host defense against *Mycobacterium bovis* Bacillus Calmette-Guerin and *Mycobacterium tuberculosis* infections. Am. J. Pathol. **166:**1109–1120.
20. **Park, J. S., M. H. Tamayo, M. Gonzalez-Juarrero, I. M. Orme, and D. J. Ordway.** 2006. Virulent clinical isolates of *Mycobacterium tuberculosis* grow rapidly and induce cellular necrosis but minimal apoptosis in murine macrophages. J. Leukoc. Biol. **79:**80–86.
21. **Riedl, S. J., and Y. Shi.** 2004. Molecular mechanisms of caspase regulation during apoptosis. Nat. Rev. Mol. Cell Biol. **5:**897–907.
22. **Riendeau, C. J., and H. Kornfeld.** 2003. THP-1 cell apoptosis in response to mycobacterial infection. Infect. Immun. **71:**254–259.
23. **Ryan, C. A., H. R. Stennicke, V. E. Nava, J. B. Burch, J. M. Hardwick, and G. S. Salvesen.** 2002. Inhibitor specificity of recombinant and endogenous caspase-9. Biochem. J. **366:**595–601.
24. **Saunders, B. M., S. Tran, S. Ruuls, J. D. Sedgwick, H. Briscoe, and W. J. Britton.** 2005. Transmembrane TNF is sufficient to initiate cell migration and granuloma formation and provide acute, but not long-term, control of *Mycobacterium tuberculosis* infection. J. Immunol. **174:**4852–4859.
25. **Schaible, U. E., F. Winau, P. A. Sieling, K. Fischer, H. L. Collins, K. Hagens, R. L. Modlin, V. Brinkmann, and S. H. E. Kaufmann.** 2003. Apoptosis facilitates antigen presentation to T lymphocytes through MHC-I and CD1 in tuberculosis. Nat. Med. **9:**1039–1046.
26. **Shiratsuchi, H., and J. J. Ellener.** 2001. Expression of IL-18 by *Mycobacterium avium*-infected human monocytes; association with *M. avium* virulence. Clin. Exp. Immunol. **123:**203–209.
27. **Slee, E. A., H. Zhu, S. C. Chow, M. MacFarlane, D. W. Nicholson, and G. M. Cohen.** 1996. Benzyloxycarbonyl-Val-Ala-Asp (OMe) fluoromethylketone (Z-VAD.FMK) inhibits apoptosis by blocking the processing of CPP32. Biochem. J. **315:**21–24.
28. **Sly, L. M., S. M. Hingley-Wilson, N. E. Reiner, and W. R. McMaster.** 2003. Survival of *Mycobacterium tuberculosis* in host macrophages involves resistance to apoptosis dependent upon induction of antiapoptotic Bcl-2 family member Mcl-1. J. Immunol. **170:**430–437.
29. **Stewart, G. R., B. D. Robertson, and D. B. Young.** 2003. Tuberculosis: a problem with persistence. Nat. Rev. Microbiol. **1:**97–105.
30. **Ulrichs, T., and S. H. E. Kaufmann.** 2006. New insights into the function of granulomas in human tuberculosis. J. Pathol. **208:**261–269.
31. **Vercammen, D., G. Brouckaert, G. Denecker, M. V. de Craen, W. Declercq, W. Fiers, and P. Vandenabeele.** 1998. Dual signaling of the Fas receptor: initiation of both apoptotic and necrotic cell death pathways. J. Exp. Med. **188:**919–930.
32. **Vercammen, D., R. Beyaert, G. Denecker, V. Goossens, G. V. Loo, W. Declercq, J. Grooten, W. Fiers, and P. Vandenabeele.** 1998. Inhibition of caspases increases the sensitivity of L929 cells to necrosis mediated by tumor necrosis factor. J. Exp. Med. **187:**1477–1485.

Editor: J. L. Flynn

Deletion of *kasB* in *Mycobacterium tuberculosis* causes loss of acid-fastness and subclinical latent tuberculosis in immunocompetent mice

Apoorva Bhatt*†‡, Nagatoshi Fujiwara§, Kiranmai Bhatt†¶, Sudagar S. Gurcha‖, Laurent Kremer**, Bing Chen*†, John Chan†, Steven A. Porcelli†, Kazuo Kobayashi§, Gurdyal S. Besra‖, and William R. Jacobs, Jr.*†,††

*Howard Hughes Medical Institute and †Department of Microbiology and Immunology, Albert Einstein College of Medicine, Bronx, NY 10461; §Department of Host Defense, Osaka City University Graduate School of Medicine, Osaka 545-8585, Japan; ‖School of Biosciences, University of Birmingham, Edgbaston, Birmingham B15 2TT, United Kingdom; and **Laboratoire de Dynamique Moléculaire des Interactions Membranaires, Centre National de la Recherche Scientifique, Unité Mixte de Recherche 5539, Université de Montpellier II, 34095 Montpellier Cedex 5, France

Edited by Barry R. Bloom, Harvard School of Public Health, Boston, MA, and approved February 1, 2007 (received for review October 2, 2006)

***Mycobacterium tuberculosis*, the causative agent of tuberculosis, has two distinguishing characteristics: its ability to stain acid-fast and its ability to cause long-term latent infections in humans. Although this distinctive staining characteristic has often been attributed to its lipid-rich cell wall, the specific dye-retaining components were not known. Here we report that targeted deletion of *kasB*, one of two *M. tuberculosis* genes encoding distinct β-ketoacyl- acyl carrier protein synthases involved in mycolic acid synthesis, results in loss of acid-fast staining. Biochemical and structural analyses revealed that the Δ*kasB* mutant strain synthesized mycolates with shorter chain lengths. An additional and unexpected outcome of *kasB* deletion was the loss of ketomycolic acid *trans*-cyclopropanation and a drastic reduction in methoxymycolic acid *trans*-cyclopropanation, activities usually associated with the *trans*-cyclopropane synthase CmaA2. Although deletion of *kasB* also markedly altered the colony morphology and abolished classic serpentine growth (cording), the most profound effect of *kasB* deletion was the ability of the mutant strain to persist in infected immunocompetent mice for up to 600 days without causing disease or mortality. This long-term persistence of Δ*kasB* represents a model for studying latent *M. tuberculosis* infections and suggests that this attenuated strain may represent a valuable vaccine candidate against tuberculosis.**

mycolic acid | Ziehl-Neelsen stain | cording | persistence | FAS-II

The Ziehl–Neelsen stain-based microscopic detection of *Mycobacterium tuberculosis*, which relies on the acid-fast attribute of the tubercle bacillus, remains the cornerstone of diagnosis of tuberculosis (TB), particularly in poor countries where the infection is highly prevalent (1). This staining method was developed by Ziehl and Neelsen who improvised on the early work of Koch, Rindfleisch, and Ehrlich (2–4). Acid-fastness has been attributed to a number of mycobacterial cell wall components, including outer lipids, arabinogalactan-bound mycolic acids (MAs), and free hydroxyl and carboxylate groups of cell wall lipids (5–7). The underlying theme in all of the proposed mechanisms was the presence of a lipid-rich, hydrophobic barrier that could be penetrated by phenol-based stains but was resistant to decolorization by acid-alcohol. However, the precise molecular component responsible for this unique staining property has never been identified.

Early studies on the effects of isoniazid on the staining characteristics of tubercle bacilli demonstrated a loss of acid-fastness after growth in the presence of the antibiotic (8). Because isoniazid was known to inhibit the synthesis of MAs, the major class of lipids composing the cell wall of mycobacteria, this result suggested that these molecules may be the components responsible for the acid-fast staining characteristic and that mutants defective in MA biosynthesis would be reasonable candidates to study the phenomenon of acid-fastness. MAs are very-long-chain α-alkyl β-hydroxy fatty acids that are either esterified to peptidoglycan-linked arabinogalactan or present as a part of the interspersed glycolipid, trehalose dimycolate (TDM) (9, 10). The long mero-MA chain is synthesized by a multienzyme fatty acid synthase II complex (FASII) from acyl carrier protein (ACP)-bound substrates that are elongated by repetitive reductive cycles, the first step of which is catalyzed by a β-ketoacyl-ACP synthase. In *M. tuberculosis* and other mycobacteria, two genes, *kasA* and *kasB*, encode distinct FASII β-ketoacyl-ACP synthases (11). Whereas *kasA* is an essential gene (12), *kasB* is not essential for normal mycobacterial growth in *Mycobacterium marinum* and *Mycobacterium smegmatis* (12, 13), suggesting that *kasB* might be an accessory gene that is not essential for MA biosynthesis. Previous *in vitro* (14) and *in vivo* (13) results had indicated that whereas KasA is involved in the initial elongation of the mero chain, KasB might be responsible for its extension to full-length mero-MAs.

Before this work, the effects of *kasB* deletion in *M. tuberculosis* were unknown, and the role of KasB in pathogenesis had not been investigated in an animal model of infection. In this work, we have shown that the deletion of *kasB* caused alterations in MAs that resulted in a loss of acid-fastness. Furthermore, the *M. tuberculosis* Δ*kasB* mutant was analyzed after infections of both immunocompromised and immunocompetent mice, which revealed a marked attenuation of *in vivo* growth in the mutant that led to a long-term persistent infection that resembled latent tuberculosis. These results provide insights into the nature of the clinically important feature of acid-fast staining in *M. tuberculosis* and are also relevant to understanding and modeling latent tuberculosis.

Results

Deletion of *kasB* Caused a Change in Mycobacterial Colony Morphology and Loss of Cording and Acid-Fastness. A specialized transducing phage, ph*ΔkasB*, containing an allelic exchange substrate designed to replace *kasB* with a hygromycin resistance cassette

Author contributions: A.B., J.C., S.A.P., G.S.B., and W.R.J. designed research; A.B., N.F., K.B., S.S.G., L.K., and B.C. performed research; K.K. and W.R.J. contributed new reagents/analytic tools; A.B., N.F., and K.B. analyzed data; and A.B. and W.R.J. wrote the paper.

The authors declare no conflict of interest.

This article is a PNAS direct submission.

Abbreviations: ACP, acyl carrier protein; FASII, fatty acid synthase II complex; MA, mycolic acid; MAME, mycolic acid methyl ester; TB, tuberculosis; TDM, trehalose dimycolate.

‡Present address: School of Biosciences, University of Birmingham, Edgbaston, Birmingham B15 2TT, United Kingdom.

¶Present address: School of Medicine, St. George's University, Grenada, West Indies.

††To whom correspondence should be addressed. E-mail: jacobsw@hhmi.org.

This article contains supporting information online at www.pnas.org/cgi/content/full/0608654104/DC1.

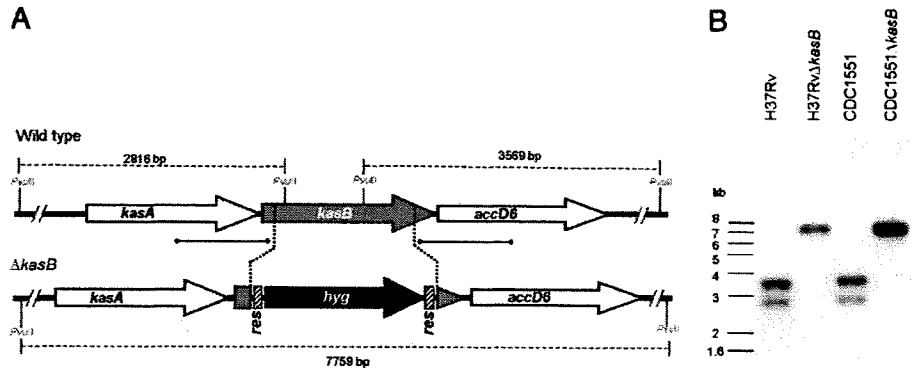

Fig. 1. Generation of a *M. tuberculosis kasB* mutant. (*A*) Map of the *M. tuberculosis kasB* region in WT and Δ*kasB* strains. [α-^{32}P]dCTP-labeled probes were derived from ≈500-bp upstream and downstream flanking sequences that were used to construct the knockout plasmids, and they are indicated by thick lines with square ends. The *PvuII*-digested fragments expected in a Southern blot are indicated by gapped lines with sizes. (*B*) Southern blot of *PvuII*-digested genomic DNA from WT and Δ*kasB* strains. Only one representative band pattern is shown for each mutant strain of H37Rv and CDC1551; *res*, $\gamma\delta$-resolvase site; *hyg*, hygromycin resistance gene.

(*hyg*), was transduced into two virulent *M. tuberculosis* strains, H37Rv (laboratory strain) and CDC1551 (clinical isolate). Southern blot analysis of genomic DNA isolated from hygromycin-resistant (Hyg^R) colonies confirmed replacement of *kasB* with *hyg* (Fig. 1). For further studies, we chose the *kasB* mutant generated in the clinical strain CDC1551; the CDC1551 parental strain, the Δ*kasB* mutant strain, and the complemented strain will be referred to here as WT (wild-type), Δ*kasB*, and Δ*kasB*(pMV261*kasB*), respectively. Deletion of *kasB* resulted in a striking alteration in colony morphology, with the mutant strain forming colonies much smaller than those of the parental strain (Fig. 2). In addition, colonies of mutant strain appeared to have a different surface texture. The smaller size of the colonies was not the result of a slower growth rate because the CDC1551 Δ*kasB* mutant had a doubling rate similar to that of its parental strain when cultured in 7H9 broth (data not shown). WT colony morphology could be restored in the Δ*kasB* mutant upon introduction of *kasB* on a multicopy-replicating plasmid (Fig. 2), indicating that the observed change was due solely to the loss of KasB and not because of a polar effect on the expression of *accD6* located downstream from *kasB*. On the other hand, no complementation was observed with a *kasA*-containing plasmid, indicating that extra copies of *kasA* could not compensate for the loss of *kasB* (data not shown).

A change in colony morphology suggested an altered cell envelope in the Δ*kasB* mutant, and a microscopic examination of cultures grown in 7H9 broth showed that the Δ*kasB* mutant was defective in cording, a classical serpentine growth (Fig. 3). A change in the cell wall composition was further confirmed by acid-fast staining of cultures by two different methods (Kinyoun stain or TB-fluorescent stain), which revealed that the Δ*kasB* strain had lost the ability to retain the primary stain after washing with the acid-alcohol decolorizer (one staining method is shown in Fig. 3). These results suggested that the change in morphology was likely due to a change in the cell wall MA content and correlated well with the increased sensitivity of the Δ*kasB* strain to the lipophilic antibiotic rifampicin (data not shown). The mutant strain was also more sensitive to the KasA/KasB inhibitor thiolactomycin [minimum inhibitory concentration (MIC) <1 μg/ml] than the WT strain (MIC = 5 μg/ml).

MA Chain Length and Cyclopropanation Are Altered in the Δ*kasB* Mutant. The changes in cording and in the acid-fast staining property of the Δ*kasB* strain prompted us to investigate the MA composition of the mutant strain. *M. tuberculosis* produces three classes of MAs: α-, keto-, and methoxy-MAs, each differing in modifications of the mero chain that are catalyzed by distinct cyclopropane synthases, isomerases, and methyl transferases

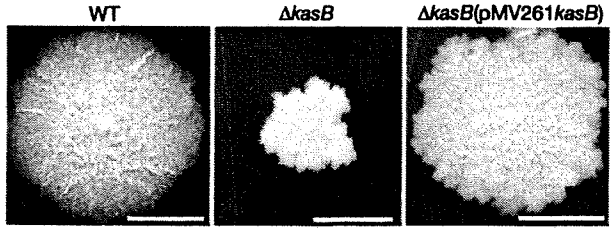

Fig. 2. Colonies of *M. tuberculosis* CDC1551 parental (WT), *kasB* null mutant (Δ*kasB*), and complemented *kasB* mutant [Δ*kasB*(pMV261*kasB*)] strains on 7H10 plates after incubation at 37°C for 4 weeks. (Scale bar, 2 mm.)

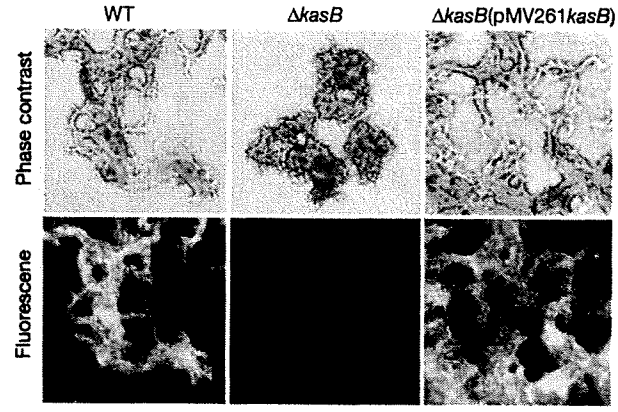

Fig. 3. Light microscopy of *M. tuberculosis* cultures grow static in 7H9 broth at 37°C for 7 days. Cultures were fixed on glass slides, and acid-fast staining was performed on the fixed smears by using the BD TB fluorescent kit-T. (*Upper*) Phase-contrast microscopy images of *M. tuberculosis* WT, Δ*kasB*, and Δ*kasB*(pMV261*kasB*) strains stained with TB-auramine-rhodamine and then treated with acid-alcohol decolorizer. (*Lower*) Fluorescent micrographs of the same fields. (Magnification, ×400.)

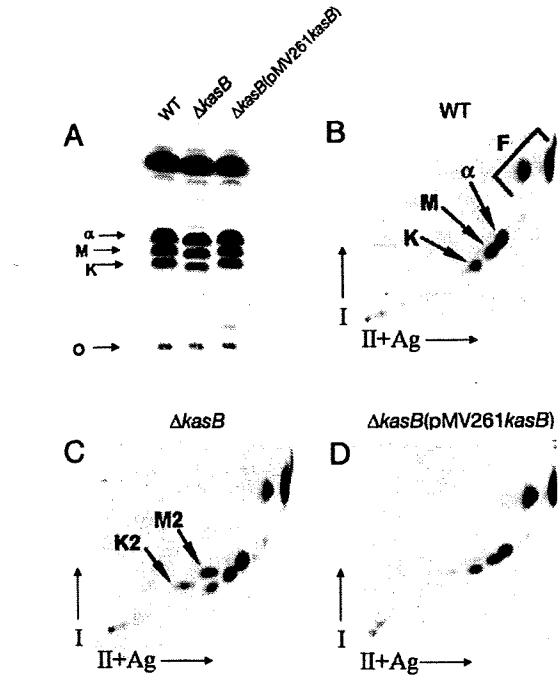

Fig. 4. TLC of ^{14}C-labeled MAMEs from *M. tuberculosis* WT, Δ*kasB*, and Δ*kasB*(pMV261*kasB*) strains. (*A*) Single-dimension HPTLC of MAMEs. (*B–D*) Two-dimensional argentation TLC of WT, Δ*kasB*, and Δ*kasB*(pMV261*kasB*), respectively. O, origin; I, first dimension; II+Ag, second dimension impregnated with $AgNO_3$; α, α-MAMEs; M, methoxy-MAMEs; K, keto-MAMEs; F, fatty acid methyl esters. The two unknown species in the Δ*kasB* strain, M2 and K2, are indicated by arrows.

(15–22). A preliminary analysis of [^{14}C]acetate-labeled MA methyl esters (MAMEs) obtained from total MAs by TLC showed that methoxy- and keto-MAMEs obtained from Δ*kasB* migrated at a slightly lower but reproducible R_f value than those from WT or complemented strains (Fig. 4*A*), suggesting a change in the MA chain lengths. Also, there were differences between the WT and mutant strain with regard to the relative abundance of the three classes of MAMEs: the relative percentages for α-, methoxy-, and keto-MAMEs in total MAMEs from WT strain were 41.5%, 33.5%, and 25%, respectively, and those for the mutant strain were 52%, 32%, and 16%, indicating a decrease in the amount of keto-MAs in the *kasB* mutant [supporting information (SI) Fig. 7]. These defects in MA composition, and the migration in TLCs, were corrected on complementation of Δ*kasB* (Fig. 4*A* and SI Fig. 7). These changes in R_f values and relative abundances of MAs were similar to those observed earlier in a *M. marinum* transposon-disrupted *kasB* mutant (13). Further analysis of MAMEs by two-dimensional argentation TLC (23) (Fig. 4 *B–D*) revealed accumulation of two spots in Δ*kasB* that migrated slightly more slowly than keto- and methoxy-MAME spots in the second dimension (M2 and K2, shown by arrows in Fig. 4*C*). The retarded migration in the second, silver-impregnated, dimension suggested that these spots corresponded to unsaturated MAME species. Similar results were obtained when MAMEs obtained from cell wall-bound MAs and extractable MAs were analyzed separately by two-dimensional TLC, indicating that the altered MAs were esterified to both arabinogalactan and to trehalose (data not shown). No changes in the profiles of other lipids (polar and apolar) were detectable on TLC plates (SI Fig. 8), indicating that the observed phenotypes of Δ*kasB* were likely due to the effects of altered MAs.

Individual MA species were purified from WT, Δ*kasB*, and Δ*kasB*(pMV261*kasB*) and analyzed by MALDI-TOF MS. Spectroscopic data revealed shortened MAs in Δ*kasB* (SI Table 1). The longest α-, methoxy-, and keto-MA species detected in the WT strain were $C_{84:2}$, $C_{92:1}$, and $C_{89:1}$, respectively, whereas in the Δ*kasB* strain the corresponding longest species were $C_{80:2}$, $C_{86:1}$, and $C_{82:1}$, respectively (SI Table 1). In addition, the chain lengths of the most abundant MA species were different in the mutant strain (SI Table 1). Detection of the α-branch by pyrolysis GC revealed that the shortening of chain length was not in the α-branch, but in the mero-MA moiety (SI Fig. 9).

The two accumulated species that were detected by two-dimensional TLC in the Δ*kasB* strain were each found to have a mass identical to the corresponding oxygenated MAME (SI Fig. 10). A more detailed study of purified MAs by ^{1}H NMR analysis revealed the presence of normal levels of *cis*-cyclopropanated methoxy-MAs but diminished resonances for *trans*-cyclopropanated methoxy-MAs in Δ*kasB* (SI Fig. 11). Additionally, no signals corresponding to *trans*-cyclopropanated keto-MAs were detected in the mutant strain (SI Fig. 11).

Furthermore, ^{1}H NMR analysis of total MAs from Δ*kasB* revealed that the two accumulated species in Δ*kasB* were unsaturated precursors of *trans*-cyclopropanated species: signals for *trans*-double bond were detected at 5.24 ppm (*J* 14.7 Hz) and at 5.34 ppm (*J* 14.7 Hz) (24), and the protons for the methylene and the methine groups adjacent to the *trans*-double bond were assigned at 1.96 ppm and 2.01 ppm (15, 25) (SI Fig. 12). The protons of the allylic methyl branch of the proximal *trans*-double bond resonated as a doublet at 0.94 ppm (*J* 6.6 Hz) and the terminal methyl at 0.84 ppm (26, 27). In contrast, spectra of total MAs from the WT strain revealed the absence of allylic methyl branch protons (0.94 ppm) and of *trans*-double bond (5.24 ppm) (data not shown). These results demonstrated that a *trans*-unsaturated precursor of both methoxy- and keto-MAs accumulated in the Δ*kasB* strain.

Loss of KasB in *M. tuberculosis* Causes a Severe Growth *in Vivo* Defect in Mice and Latent Subclinical TB. To assess the effects of altered MAs in the Δ*kasB* strain on mycobacterial virulence, we first tested the ability of the Δ*kasB* mutant to survive in murine (C57BL/6 bone marrow-derived and J774) macrophages and THP-1 cells and found no differences between WT and Δ*kasB* (data not shown). Next, immunocompetent C57BL/6 mice were infected with aerosols of WT, Δ*kasB*, and complemented strains (≈100 bacteria per mouse). Extensive granulomatous inflammation was visible in the lungs of mice infected with the WT or Δ*kasB*(pMV261*kasB*) strains but not in those infected with the Δ*kasB* strain (Fig. 5*A*). Histological examination of stained lung sections from mice infected with the WT or Δ*kasB*(pMV261*kasB*) strains revealed multifocal, moderate infiltration after 21 days of infection (Fig. 5*B*). The severity of the granulomatous lesions increased after 56 days, and after 112 days there was coalescence of lesions into large areas that involved entire lobes of the lung. In contrast, the lungs of mice infected with Δ*kasB* showed more diffuse and less organized infiltrates at 21 days, which decreased in severity after 56 days, and no signs of infection were seen after 112 days (Fig. 5*B*). Consistent with the loss of acid-fastness observed for broth cultures, the *kasB* mutant also failed to retain the primary stain in tissue sections after acid-fast staining and instead took up the methylene blue counterstain (SI Fig. 13).

Monitoring of colony-forming units (cfu) in the lung, spleen, and liver at different time points after infection indicated that the Δ*kasB* mutant was severely attenuated for growth in mice. WT bacteria could replicate extensively in the lung in the first 21 days after aerosol infection, with a three log increase in WT bacteria in infected lungs at the end of 21 days (Fig. 6*A*). In contrast, replication of the Δ*kasB* strain was restricted: bacterial loads in the lung barely increased by 2 orders of magnitude after 21 days of infection and then decreased to between 500 and 1,000

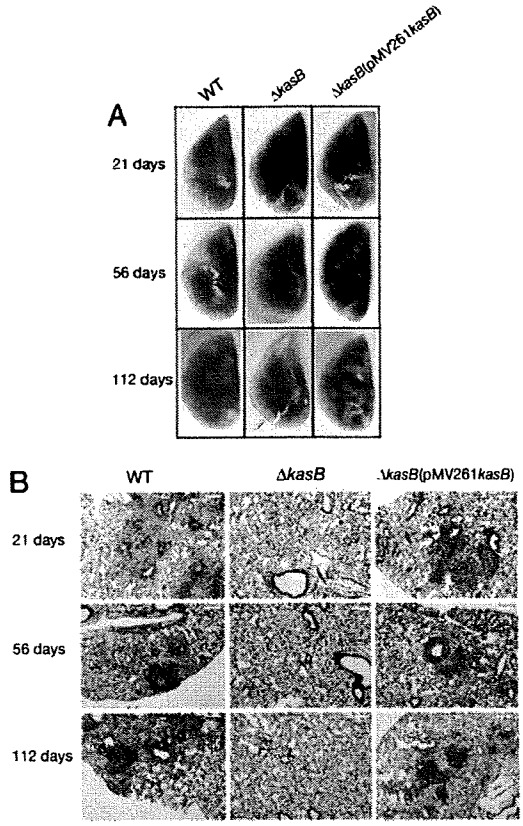

Fig. 5. Pathology of infected mouse lungs. (*A*) Lungs of C57BL/6 mice infected with *M. tuberculosis* WT, Δ*kasB*, and Δ*kasB*(pMV261*kasB*) strains, removed at different time points after aerosol infection. (*B*) Hematoxylin/eosin-stained lung tissue sections from mice infected with WT, Δ*kasB*, or Δ*kasB*(pMV261*kasB*). (Scale bar, 200 μm.)

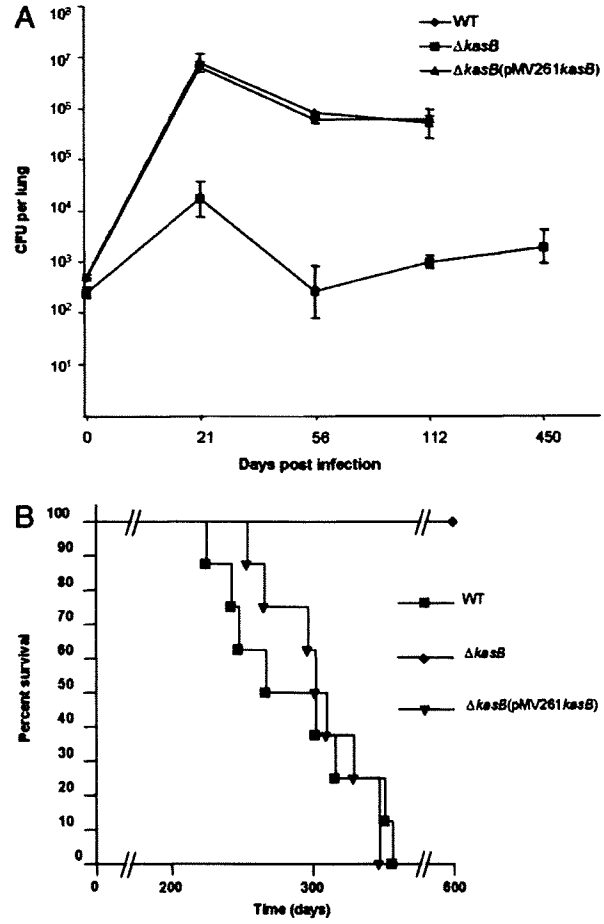

Fig. 6. Attenuation of Δ*kasB* in C57BL/6 mice. (*A*) Plot of *M. tuberculosis* cfu levels in lungs of C57BL/6 mice at different time points after aerosol infection. (*B*) Survival curve of C57BL/6 mice infected with WT, Δ*kasB*, or Δ*kasB* (pMV261*kasB*).

cfu in subsequent weeks (Fig. 6*A*). The Δ*kasB* mutant was also attenuated for growth in liver and spleen (SI Fig. 14 *A* and *B*). Surprisingly, 450 days after aerosol infection, ≈1,000 cfu could still be detected in the lungs of Δ*kasB*-infected mice (Fig. 6*A*), although the mice looked healthy before being killed, which indicated that the mutant was able to persist in the mouse without causing visible signs of disease. Indeed, we observed a significant difference in the mortality of C57BL/6 mice infected by aerosols of the CDC1551 strains (100 cfu per mouse). By day 356, 100% (eight of eight) of the mice infected with WT or Δ*kasB*(pMV261*kasB*) had died (Fig. 6*B*). In stark contrast, all mice infected with Δ*kasB* (eight of eight) were not only alive but also appeared healthy even after 600 days after infection, indicating that Δ*kasB* had failed to cause active infection in the mice. Surprisingly, unlike the results obtained with C57BL/6 mice, the Δ*kasB* strain caused mortality in immunodeficient SCID mice (SI Fig. 15).

Discussion

Our studies demonstrate that the FASII β-ketoacyl-ACP synthase KasB is essential for full MA chain length in *M. tuberculosis*. Although the results of *in vitro* assays suggested that KasB may be involved in elongating a major portion of the mero-MA chain (14), deletion of *kasB* resulted in the shortening of the mero-MA chains by only 2–6 carbons. In addition, the Δ*kasB* mutant lost the ability to synthesize any *trans*-cyclopropanated keto-MAs and produced a miniscule amount of *trans*-cyclopropanated methoxy-MAs, accumulating instead their corresponding unsaturated precursors with *trans*-double bonds, which are putative substrates of the *trans*-cyclopropane synthase CmaA2 (18). This unexpected consequence of *kasB* deletion meant that either the shortened oxygenated mero-MAs are poor substrates for CmaA2 or that CmaA2 interacts preferentially with KasB present in specialized FASIIs, as recently suggested (28, 29). Thus, the deletion of *kasB* had a "downstream phenotypic" effect on *trans*-cyclopropanation of oxygenated MAs, an activity not directly associated with KasB function. In addition, the proportions of the different MA species were also altered, with a reduction in the levels of keto-MAs. These alterations in structure (shortening of MA chain length and loss or reduction of *trans*-cyclopropanation) and in content (reduction in keto-MAs) were observed for both wall-bound and trehalose-bound MAs (data not shown).

Our findings have similarities but also several differences compared with those reported for a transposon-disrupted *kasB* mutant of *M. marinum* (13). In that study, MA species 4 carbons shorter were found compared with up to 6 carbons shorter in the *M. tuberculosis* mutant. We also observed that the deletion of *kasB* affected MA *trans*-cyclopropanation, an activity not detected in WT *M. marinum*. And finally, unlike the *M. marinum* mutant study, we were able to test the ability of the *M. tuberculosis* Δ*kasB* mutant to cause infection in an animal model of infection and thus assess the role of KasB in virulence.

A remarkable change in Δ*kasB* was the complete loss of the acid-fast staining property that is one of the primary defining characteristics of *M. tuberculosis*. Loss of acid-fastness by Δ*kasB* was not only observed in broth cultures but also in infected murine lung tissue. Here again, direct or indirect effects of changes in the MAs of the *kasB* mutant, like a decrease in lipophilicity, may have rendered the cell wall more prone to decolorization with acid-alcohol. It is unlikely that any specific chemical interactions of MAs with the primary stain that were lost in Δ*kasB* could have been responsible for the loss of acid-fastness because two different staining methods (using chemically distinct primary stains) yielded the same results. This work reports the loss of acid-fastness in a specific *M. tuberculosis* mutant that is defective in normal MA biosynthesis, and the only other well characterized acid-fast negative *M. tuberculosis* mutant described has a deletion in *phoP*, which leads to deficiencies of many lipids, including sulfatides, diacyltrehaloses, and polyacyltrehaloses (30). It is worth noting that the deletion of *cmaA2* in *M. tuberculosis* did not alter colony morphology, cording, or acid-fastness (18), indicating that loss of or reduction in *trans*-cyclopropanation can be ruled out as a potential cause of the observed phenotypes in Δ*kasB*.

TDMs are believed to play a particularly important role in determining colony characteristics and cording (31), and the observed changes in colony morphology and cording in the Δ*kasB* mutant were thus likely a direct or indirect effect of the altered MA profile of the TDMs produced by the mutant. Loss of cording is often associated with decreased virulence (19), and indeed this was the case with the Δ*kasB* mutant. Before these studies, three other *M. tuberculosis* mutants defective in MA biosynthesis had been tested in the mouse model of infection: Δ*mma4* and Δ*pcaA* were found to be attenuated (16, 19), whereas Δ*cmaA2* was hypervirulent (32). Although Δ*pcaA* and Δ*mmaA4* showed reduced replication in mouse organs, moderately high numbers of bacteria could be found in the lungs, spleen, and liver of mice even 20–30 weeks after infection (albeit lower than those found for the WT strain) (16, 19). None of these three mutants has been reported as acid-fast negative, and only the Δ*pcaA* mutant was defective in cording.

The Δ*kasB* mutant displayed a number of interesting *in vivo* phenotypes. First, it was severely attenuated for growth in immunocompetent C57BL/6 mice: the mutant did initially colonize lung, liver, and spleen in infected immunocompetent C57BL/6 mice; determination of bacterial loads in organs and histological examination of tissue sections revealed that Δ*kasB* failed to replicate to the levels normally observed in these tissues and did not cause the pathology usually associated with *M. tuberculosis* infection.

Perhaps the most striking *in vivo* phenotype of the Δ*kasB* mutant was its ability to persist at constant low levels in lungs and spleen for 450 days after aerosol infection. The mutant also failed to cause active disease in the mice: Δ*kasB*-infected mice appeared healthy even 600 days after infection. In contrast, SCID mice succumbed to infection by Δ*kasB*, indicating a clear role for cell-mediated immunity in the control of replication of the Δ*kasB* mutant. The absence of any differences between WT and Δ*kasB* in regard to their ability to survive in macrophages suggests that early defense mechanisms, like intracellular oxidative damage in macrophages, did not play a role in the attenuation of the mutant strain. Thus, the surprising "hypovirulence" of Δ*kasB* could be a consequence of a number of other factors resulting from the altered MA profile and their effects on the interaction of the bacteria with the host adaptive immune system. One possibility is the exposure of cell envelope components, normally "masked" in WT strains, which may induce a more robust immune response. Another possibility is the modulation of the immune response by cell wall components; TDMs are the major cell wall glycolipids and are known to modulate the immune response (32, 33). It is therefore likely that Δ*kasB* TDMs containing altered MAs modulate innate and adaptive immune responses, resulting in the observed *in vivo* growth defect.

A third of the human population is latently infected with the tubercle bacillus, and this dormant, drug-tolerant stage of the bacterium is a major challenge for the tuberculosis therapy and control. Although this latency provides an important reservoir for disease reactivation, very little is known about bacterial and host factors that are involved in long-term persistence. The long-term persistence of Δ*kasB* for up to 600 days in immunocompetent mice without causing disease suggests that the mutant strain can provide a good model for studying latent *M. tuberculosis* infection. Furthermore, this unique *in vivo* phenotype makes *kasB* an attractive candidate for deletion in a live attenuated vaccine strain.

The increased sensitivity of the *kasB* mutant to lipophilic antibiotics highlights the attractiveness of KasB as an important secondary drug target in combination therapy. Specific inhibitors of KasB could be envisioned as inhibiting long-chain mero-MA biosynthesis and, as a result, attenuating *M. tuberculosis* while at the same time making the bacterium even more susceptible to drugs such as rifampicin used in combination. In addition to an increased permeability to lipophilic drugs, the increased sensitivity of Δ*kasB* to thiolactomycin, a drug known to inhibit both KasA and KasB (34), may have been due to a lesser titration of the drug as a result of the absence of KasB.

In summary, our studies have demonstrated that KasB-mediated elongation of MAs is crucial for cording, acid-fast staining, subsequent *trans*-cyclopropanation, and the ability of *M. tuberculosis* to cause disease in immunocompetent mice. Our findings have important implications for understanding and solving the problems of latency and antibiotic tolerance in *M. tuberculosis* infection.

Materials and Methods

Plasmids and Phages. Plasmids and phages used in this work are outlined in SI Table 2. Slow-growing mycobacteria were cultured in 7H9 broth (Difco, Sparks, MD) containing 10% Middlebrook OADC enrichment and 0.05% Tween 80, on 7H9 agar (made by adding 1.5% agar to OADC-enriched 7H9 broth), or on Middlebrook 7H10 agar (Difco). *Escherichia coli* strains were cultured in LB broth. The concentrations of antibiotics used were 75 μg/ml hygromycin and 20 μg/ml kanamycin for mycobacterial strains, and 150 μg/ml hygromycin and 40 μg/ml kanamycin for *E. coli*.

Construction of Deletion Mutants. For generating an allelic exchange construct designed to replace the *kasB* gene with a hygromycin resistance cassette (*hyg*), 500-bp sequences flanking the left and right of the *M. tuberculosis kasB* gene were PCR-amplified from pYUB2271 (a cosmid vector containing *kasB*) using the primer pairs MtKasB1 (5′-GCGACTAGTGGTAGGGCGATGACTCGC-3′) and MtKasB2 (5′-CGTATGCATACCAGCTCCGTCATTG-3′), and MtKasB3 (5′-GCGTCTAGAGAGATCGATTTGGACGTG-3′) and MtKasB4 (5′-GCAGGTACCACCGAGATCTGCGGGATG-3′), respectively. After cloning into pCR2.1-TOPO and sequencing, the cloned PCR fragments were excised by using the primer-introduced restriction sites and cloned into the allelic exchange plasmid vector pJSC347 (SI Table 2). The resultant plasmid, pYUB2417, was then packaged into the temperature-sensitive phage phAE159 (J. Kriakov and W.R.J., Jr., unpublished results), as described (35), to yield the *kasB*-knockout phage phAE404. Specialized transduction was performed as described (35).

Biochemical Analyses of MAs and Lipids. TLC analysis of MAs was done as described (23, 34). MA extraction and derivatization for TLC analysis, and purification for MS and NMR analysis, were

done as described (19, 36). In brief, MAs of each strain were liberated by alkali hydrolysis (10% KOH/methanol, wt/vol) from the heat-killed bacteria at 90°C for 2 h, followed by extraction with *n*-hexane. After methylation with diazomethane, each subclass, α-, methoxy-, and keto-MAME, was purified by preparative TLC of silica gel until a single spot was obtained. The developing system was benzene or *n*-hexane/diethyl ether (90:15, vol/vol). The molecular species of the MAMEs were detected by MALDI-TOF MS by using an Ultraflex II (Bruker Daltonics, Billerica, MA). The purified MAMEs were prepared in chloroform at a concentration of 1 mg/ml, and a droplet of a 1-μl sample was applied directly on the sample plate followed by 1 μl of matrix solution (2,5-dihydroxybenzoic acid/10 mg/ml in chloroform/methanol, 1:1 vol/vol). MAMEs were analyzed in the Reflectron mode with an accelerating voltage operating in positive mode of 20 kV. An external mass calibration was performed by peptide calibration standard II (Bruker Daltonics), including known peptide standards in a mass range from 700 to 4,000 Da (15). ^{1}H NMR spectra of MAMEs were obtained in $CDCl_3$ (100% D) by using a Bruker Avance 600 spectrometer at 25°C. Chemical shift values (in ppm) were relative to internal $CHCl_3$ resonance (at 7.26 ppm). Pyrolysis and subsequent GC-MS of MAs was done in accordance with published methods (37, 38). Lipid extraction and TLC analysis were done as described (39).

Mouse Infections. C57BL/6 mice were exposed to aerosols of different strains of *M. tuberculosis* in an aerosolization chamber. A suspension of 10^6 cfu/ml in PBS containing 0.05% Tween 80 and 0.004% antifoam was used as the inoculum to obtain ≈100 cfu per lung. Four mice from each infection group were killed 24 h after infection, and lung homogenates were plated on 7H9-agar plates to determine the efficiency of aerosolization. At different time points, three or four mice were killed from each infection group to determine bacterial loads in the spleen, lung, and liver. Eight mice from each group were also used to determine survival times of infected mice. Pathological analysis and histological staining of organ sections were done on tissues fixed in buffered 10% formalin.

We thank Annie Dai, Mei Chen, and John Kim for technical assistance; Jordan Kriakov (Albert Einstein College of Medicine) for providing phAE159; Howard Steinman for helpful comments; and Matsumi Doe, Shinji Maeda, and Takashi Naka of Osaka City University for technical support. This work was supported by Howard Hughes Medical Institute and National Institutes of Health Grants AI063537 (to W.R.J.) and AI26170 (to W.R.J., S.A.P and J.C.); Center for AIDS Research Grant AI051519; Grants H12-Shinko-30, H16-Shinko-1 and H18-Shinko-11 from the Ministry of Health, Labor, and Welfare in Japan (to N.F. and K.K.); a grant from the Medical Research Council and the Wellcome Trust, U.K. (to G.S.B.); and Centre National de la Recherche Scientifique CNRS ATIP "Microbiologie Fondamentale" (to L.K.). G.S.B. acknowledges support from Mr. James Bardrick in the form of a Personal Research Chair, and as a former Lister Institute-Jenner Research Fellow. A.B. acknowledges support from the Medical Research Council (U.K.) in the form of Career Development Award G0600105 at the University of Birmingham.

1. Trebucq A (2004) *Int J Tuberc Lung Dis* 8:805.
2. Bishop PJ, Neumann G (1970) *Tubercle* 51:196–206.
3. Neelsen F (1883) *Centralbl Med Wissen* 28:497.
4. Ziehl F (1882) *Deut Med Wochen* 8:451.
5. Goren MB, Cernich M, Brokl O (1978) *Am Rev Respir Dis* 118:151–154.
6. Harada K (1976) *Stain Technol* 51:255–260.
7. Murohashi T, Kondo E, Yoshida K (1969) *Am Rev Respir Dis* 99:794–798.
8. Koch-Weser D, Barclay WR, Ebert RH (1955) *Am Rev Tuberc* 71:556–565.
9. Besra GS, Sievert T, Lee RE, Slayden RA, Brennan PJ, Takayama K (1994) *Proc Natl Acad Sci USA* 91:12735–12739.
10. Brennan PJ, Nikaido H (1995) *Annu Rev Biochem* 64:29–63.
11. Cole ST, Brosch R, Parkhill J, Garnier T, Churcher C, Harris D, Gordon SV, Eiglmeier K, Gas S, Barry CE, III, *et al.* (1998) *Nature* 393:537–544.
12. Bhatt A, Kremer L, Dai AZ, Sacchettini JC, Jacobs WR, Jr (2005) *J Bacteriol* 187:7596–7606.
13. Gao LY, Laval F, Lawson EH, Groger RK, Woodruff A, Morisaki JH, Cox JS, Daffe M, Brown EJ (2003) *Mol Microbiol* 49:1547–1563.
14. Slayden RA, Barry CE, III (2002) *Tuberculosis* 82:149–160.
15. Dinadayala P, Laval F, Raynaud C, Lemassu A, Laneelle MA, Laneelle G, Daffe M (2003) *J Biol Chem* 278:7310–7319.
16. Dubnau E, Chan J, Raynaud C, Mohan VP, Laneelle MA, Yu K, Quemard A, Smith I, Daffe M (2000) *Mol Microbiol* 36:630–637.
17. Glickman MS (2003) *J Biol Chem* 278:7844–7849.
18. Glickman MS, Cahill SM, Jacobs WR, Jr (2001) *J Biol Chem* 276:2228–2233.
19. Glickman MS, Cox JS, Jacobs WR, Jr (2000) *Mol Cell* 5:717–727.
20. Takayama K, Wang C, Besra GS (2005) *Clin Microbiol Rev* 18:81–101.
21. Yuan Y, Barry CE, III (1996) *Proc Natl Acad Sci USA* 93:12828–12833.
22. Yuan Y, Crane DC, Musser JM, Sreevatsan S, Barry CE, III (1997) *J Biol Chem* 272:10041–10049.
23. Kremer L, Guerardel Y, Gurcha SS, Locht C, Besra GS (2002) *Microbiology* 148:3145–3154.
24. George KM, Yuan Y, Sherman DR, Barry CE, III (1995) *J Biol Chem* 270:27292–27298.
25. Watanabe M, Aoyagi Y, Ridell M, Minnikin DE (2001) *Microbiology* 147:1825–1837.
26. Astola J, Munoz M, Sempere M, Coll P, Luquin M, Valero-Guillen PL (2002) *Microbiology* 148:3119–3127.
27. Watanabe M, Ohta A, Sasaki S, Minnikin DE (1999) *J Bacteriol* 181:2293–2297.
28. Veyron-Churlet R, Bigot S, Guerrini O, Verdoux S, Malaga W, Daffe M, Zerbib D (2005) *J Mol Biol* 353:847–858.
29. Veyron-Churlet R, Guerrini O, Mourey L, Daffe M, Zerbib D (2004) *Mol Microbiol* 54:1161–1172.
30. Walters SB, Dubnau E, Kolesnikova I, Laval F, Daffe M, Smith I (2006) *Mol Microbiol* 60:312–330.
31. Hunter RL, Venkataprasad N, Olsen MR (2006) *Tuberculosis* 86:349–356.
32. Rao V, Gao F, Chen B, Jacobs WR, Jr, Glickman MS (2006) *J Clin Invest* 116:1660–1667.
33. Rao V, Fujiwara N, Porcelli SA, Glickman MS (2005) *J Exp Med* 201:535–543.
34. Kremer L, Douglas JD, Baulard AR, Morehouse C, Guy MR, Alland D, Dover LG, Lakey JH, Jacobs WR, Jr, Brennan PJ, *et al.* (2000) *J Biol Chem* 275:16857–16864.
35. Bardarov S, Bardarov S, Jr, Pavelka MS, Jr, Sambandamurthy V, Larsen M, Tufariello J, Chan J, Hatfull G, Jacobs WR, Jr (2002) *Microbiology* 148:3007–3017.
36. Fujiwara N, Pan J, Enomoto K, Terano Y, Honda T, Yano I (1999) *FEMS Immunol Med Microbiol* 24:141–149.
37. Guerrant GO, Lambert MA, Moss CW (1981) *J Clin Microbiol* 13:899–907.
38. Kaneda K, Imaizumi S, Yano I (1995) *Microbiol Immunol* 39:563–570.
39. Dobson G, Minnikin DE, Minnikin SM, Parlett M, Goodfellow M, Ridell M, Magnusson M (1985) in *Chemical Methods in Bacterial Systematics*, eds Goodfellow M, Minnikin DE (Academic, London), pp 237–265.

JOURNAL OF BACTERIOLOGY, Nov. 2007, p. 8241–8249 Vol. 189, No. 22
0021-9193/07/$08.00+0 doi:10.1128/JB.00550-07

Control of Cell Wall Assembly by a Histone-Like Protein in Mycobacteria[▽]

Tomoya Katsube,[1,2] Sohkichi Matsumoto,[1]* Masaki Takatsuka,[1,2] Megumi Okuyama,[1] Yuriko Ozeki,[3] Mariko Naito,[4] Yukiko Nishiuchi,[1] Nagatoshi Fujiwara,[1] Mamiko Yoshimura,[1] Takafumi Tsuboi,[5] Motomi Torii,[6] Nobuhide Oshitani,[2] Tetsuo Arakawa,[2] and Kazuo Kobayashi[7]

Department of Host Defense[1] and Department of Gastroenterology,[2] Osaka City University Graduate School of Medicine, 1-4-3 Asahi-machi, Abeno-ku, Osaka 545-8585, Japan; Sonoda Women's University, 7-29-1 Minamitsukaguchi-cho, Amagasaki, Hyogo, Japan[3]; Division of Microbiology and Oral Infection, Department of Molecular Microbiology and Immunology, Nagasaki University Graduate School of Biomedical Sciences, 1-7-1 Sakamoto, Nagasaki 852-8588, Japan[4]; Cell-Free Science and Technology Research Center and Venture Business Laboratory, Ehime University, 3 Bunkyo-cho, Matsuyama, Ehime 790-8577, Japan[5]; Department of Molecular Parasitology, Ehime University Graduate School of Medicine, Toon, Ehime 791-0295, Japan[6]; and Department of Immunology, National Institute of Infectious Diseases, Toyama 1-23-1, Shinjuku-ku, Tokyo 162-8640, Japan[7]

Received 11 April 2007/Accepted 1 September 2007

Bacteria coordinate assembly of the cell wall as well as synthesis of cellular components depending on the growth state. The mycobacterial cell wall is dominated by mycolic acids covalently linked to sugars, such as trehalose and arabinose, and is critical for pathogenesis of mycobacteria. Transfer of mycolic acids to sugars is necessary for cell wall biogenesis and is mediated by mycolyltransferases, which have been previously identified as three antigen 85 (Ag85) complex proteins. However, the regulation mechanism which links cell wall biogenesis and the growth state has not been elucidated. Here we found that a histone-like protein has a dual concentration-dependent regulatory effect on mycolyltransferase functions of the Ag85 complex through direct binding to both the Ag85 complex and the substrate, trehalose-6-monomycolate, in the cell wall. A histone-like protein-deficient *Mycobacterium smegmatis* strain has an unusual crenellated cell wall structure and exhibits impaired cessation of glycolipid biosynthesis in the growth-retarded phase. Furthermore, we found that artificial alteration of the amount of the extracellular histone-like protein and the Ag85 complex changes the growth rate of mycobacteria, perhaps due to impaired down-regulation of glycolipid biosynthesis. Our results demonstrate novel regulation of cell wall assembly which has an impact on bacterial growth.

Bacteria organize biogenesis of the cell wall as well as synthesis of cellular components depending on the growth state. However, factors linking the growth state and cell wall biogenesis have not been identified.

Mycobacterium tuberculosis is a top killer among bacterial pathogens and is responsible for 2 million deaths annually (6). *M. tuberculosis* can be quiescent in host cells for a long period of time, growing very slowly or present in a dormant state without multiplication, and it latently infects one-third of the world's human population (22, 43). In 5 to 10% of infected hosts the bacterium reactivates and causes progressive disease during their lifetimes. Most cases of active tuberculosis do not result from the initial infection but instead represent reactivation of previously implanted bacteria (22, 43).

The cell wall is critical for long-term persistence of *M. tuberculosis* in the hostile environment in the host cells and for progression of tuberculosis (3, 7). Mycobacteria are gram-positive bacilli, but the cell wall structures are different from those of other gram-positive bacteria. Approximately one-half of the cell wall mass is comprised of large (C_{70} to C_{90}) branched-chain fatty acids called mycolic acids. Mycolic acids are distributed in acid-fast positive bacteria, such as *Mycobacterium*, *Corynebacterium*, *Rhodococcus*, and *Nocardia*, although mycobacterial mycolic acids are the longest mycolic acids and have the largest side chains (C_{20} to C_{24}). The cell wall outer layer is composed of extractable glycolipids containing mycolic acids, such as trehalose-6-monomycolate (TMM) and trehalose-6,6′-dimycolate (TDM) (also called cord factor), while the inner layer is composed of mycolic acids covalently linked to the distal portion of the arabinogalactan (AG) moiety (7). TMM- or TDM-derived mycolic acids are transferred to other TMM to synthesize TDM and also to peptidoglycan-linked AG to construct the inner layer of the envelope. Antigen 85 (Ag85) complex proteins (Ag85A, Ag85B, and Ag85C) are mycolyltransferases and catalyze transfer of mycolic acids to free trehalose, TMM, and TDM (4). Ag85 complex proteins are also believed to catalyze the transfer of mycolic acids from TMM or TDM to peptidoglycan-linked AG, because inactivation of Ag85C reduced the level of AG-linked mycolic acids (16).

Regulatory proteins involved in cell wall assembly should localize in the mycobacterial cell wall. We and other groups found that a histone-like DNA-binding protein, which was designated mycobacterial DNA-binding protein 1 (MDP1), laminin-binding protein, histone-like protein (HLP), or HupB, not only localizes in the cytoplasmic space but also occurs externally or is in the mycobacterial cell wall (26, 36, 38).

* Corresponding author. Mailing address: Department of Host Defense, Osaka City University Graduate School of Medicine, 1-4-3 Asahi-machi, Abeno-ku, Osaka 545-8585, Japan. Phone: 81-6-6645-3746. Fax: 81-6-6645-3747. E-mail: sohkichi@med.osaka-cu.ac.jp.

▽ Published ahead of print on 14 September 2007.

MDP1 is mycobacterium-specific histone-like protein. *M. tuberculosis* has a single *mdp1* gene (Rv2986c, also called *hupB*) (9, 13), and the *mdp1* gene is conserved even in *Mycobacterium leprae*, which lost many genes during evolution (10). MDP1 likely plays a significant role in DNA functions in mycobacteria, as a transposon-based screen suggested that *mdp1* is essential in *M. tuberculosis* (34). However, the *mdp1* gene can be knocked out in *Mycobacterium smegmatis*, suggesting that another DNA-binding protein may compensate for loss of MDP1 in *M. smegmatis*. The *M. smegmatis* MDP1 knockout (KO) strain exhibited growth kinetics similar to those of the wild type in anaerobic culture (19) but was unable to resume growth at 10°C (37), suggesting that MDP1 plays an important role during stress responses in *M. smegmatis*.

Accumulation of MDP1 in stationary phase or under anaerobic conditions implies that MDP1 is a possible factor that participates in growth-state-dependent regulation of cell wall assembly through binding to sacchariferous components, such as glycolipids, in the cell wall. Based on this hypothesis, here we examined the physiological role of MDP1 in the cell wall.

MATERIALS AND METHODS

Extraction and purification of glycolipids. *M. tuberculosis* H37Rv and *Mycobacterium bovis* bacillus Calmette-Guérin (BCG) were cultivated on Sauton medium at 37°C. *M. smegmatis* was cultured in Luria-Bertani (LB) medium at 37°C. Bacteria were autoclaved for 10 min, disrupted ultrasonically, and then suspended in chloroform-methanol (4:1, 3:1, or 2:1, vol/vol) to extract lipids. The chloroform layer was collected and dried. TDM was first partially purified by precipitation with acetone, chloroform-methanol (2:1, vol/vol), and tetrahydrofuran-methanol (1:2, vol/vol), followed by passage through a column of silica gel (Wakogel C-200; Wako Pure Chemical, Osaka, Japan) with chloroform-methanol (4:1, vol/vol). The purity of TDM was demonstrated by a single spot on a thin-layer chromatogram. TMM was separated by preparative thin-layer chromatography (TLC) on a silica gel plate (Uniplate; 20 by 20 cm; 250 mm; Analtech, Inc., Newark, DE) using a chloroform-methanol-acetone-acetic acid (80:20:6:1, vol/vol/vol/vol) solvent system. Glycolipids were visualized with a 20% H_2SO_4 spray, followed by charring at 200°C for analytical purposes or with iodine vapor for a few minutes for preparative purposes. TMM was recovered from the plate immediately after the iodine color had disappeared by passing the plate through a small glass column with the solvent chloroform-methanol (2:1, vol/vol). Finally, TMM was purified until a single spot was obtained by repeating TLC.

Fluorescence microscopy. MDP1 was purified from BCG by using a method described previously (26). Egg white lysozyme was purchased from Wako. Bovine histone H1 was purchased from Roche Diagnostics. Proteins were labeled with 5(6)-carboxyfluorescein-*N*-hydroxysuccinimide ester (FLUOS) by using a fluorescein protein labeling kit (Roche Diagnostics) according to the manufacturer's instructions. BCG was grown in Middlebrook 7H9-ADC medium at 37°C until the optical density at 600 nm (OD_{600}) was 1.5; then it was collected by centrifugation and washed three times with phosphate-buffered saline (PBS) with 10% fetal bovine serum (FBS). FLUOS-labeled proteins, such as MDP1 (50 μg), egg white lysozyme (38 μg), and bovine histone H1 (50 μg), were added to the BCG suspension and incubated at 37°C for 30 min. BCG was washed three times with PBS with 10% FBS and then mounted on a microscope slide and viewed with a confocal scanning laser microscope (LSM510; Carl Zeiss).

MAb preparation. Ten micrograms of MDP1 and 10 ng of *M. tuberculosis* DNA were mixed in PBS, emulsified in Freund's incomplete adjuvant, and injected into BALB/c mice subcutaneously (24). Two weeks later, the mice were boosted in the same way; after an additional 2 weeks, the mice were again boosted by injection of 10 μg of MDP1 in PBS into the tail vein. Three days after the final boost, mice were sacrificed and splenocytes were obtained. A monoclonal antibody (MAb) was prepared essentially as described by Harlow and Lane (15) and was screened by an enzyme-linked immunosorbent assay (ELISA) as described below. After an initial screening, several hybridoma cell lines were cloned by two rounds of limiting dilution. A selected subclone was expanded for freezing and for ascites production in pristane-primed mice. The subclass of the hybridoma subclone was determined with a mouse MAb isotyping kit (Amersham). Immunoglobulins (Ig) were purified from ascites fluid by using an Ampure PA kit (Amersham).

ELISA to detect interactions between MDP1 and TDM, TMM, mycolic acids, or Ag85 complex proteins. TMM, TDM, and mycolic acid methyl esters (MAMEs) purified from *M. tuberculosis* Aoyama B were purchased from Nakarai and dissolved in *N*-hexane at a concentration of 50 μg/ml. Glycolipids were immobilized on a 96-well ELISA plate (Sumitomo, Osaka, Japan) by adding 100 μl of glycolipid solution and dried. Ag85A, Ag85B, and Ag85C derived from *M. tuberculosis* H37Rv and bovine serum albumin (BSA) were immobilized on the 96-well ELISA plate (Sumitomo, Osaka, Japan) by incubation of serial twofold dilutions of the protein solutions in sodium bicarbonate buffer (pH 9.6) at 4°C overnight. MDP1 at a concentration of 1 μg/ml in PBS containing 0.05% Tween 20 (PBS-T) was added to wells and incubated for 1 h at 37°C. The wells were washed with PBS-T four times, and then MAb 3A was added. After incubation at 37°C for 1 h, the wells were washed, peroxidase-conjugated anti-mouse antibody (Dako) diluted 1:2,000 was added, and the plate was incubated for 1 h. After the wells were washed, the level of MDP1 binding was detected by color development with *o*-phenylenediamine dihydrochloride (Wako, Tokyo, Japan) and measuring the OD_{492}.

Preparation of subcellular fractions. Subcellular fractions were prepared by a method described previously (1, 27). Briefly, after BCG and *M. smegmatis* were cultured in Sauton medium and LB medium, respectively, bacteria were collected by centrifugation at 10,000 × *g* and suspended in ice-cold PBS. The bacteria were then disrupted with a Bioruptor UCD-200T sonicator (Toso), and each suspension was centrifuged at 3,000 × *g* for 5 min to remove unbroken bacteria. The supernatant was used as the total cellular fraction. The total cellular fraction was fractionated further to obtain a cell wall fraction and a non-cell-wall fraction using the following procedure. The total cellular fraction was centrifuged at 10,000 × *g* for 10 min. The pellet was rinsed with cold PBS and centrifuged again at 10,000 × *g* for 10 min. The supernatants were designated the non-cell-wall fraction. The cell wall-containing pellet was suspended again in ice-cold PBS, and then Percoll (Amersham Biosciences) was added to a concentration of 60% and mixed by vortexing. Next, the cell wall-containing fraction was centrifuged at 27,000 × *g* for 1 h to separate the cell walls from the unbroken cells completely. The cell wall band was collected and washed twice with PBS, and it was designated the cell wall fraction.

Immunoprecipitation assay. Cell walls derived from BCG as described above were precleaned by using 25 μg of mouse IgG (Chemicon International Temecula) or rabbit Ig in 100 μl of protein G-coupled Sepharose (Amersham Pharmacia Biotech), incubated at 4°C for 2 h, and centrifuged. The supernatants were colleted and incubated with 250 μg of anti-MDP1 MAb 3A, control mouse IgG, anti-Ag85 Ig, or control rabbit Ig at 4°C for 16 h, and then 300 μl of protein G-coated Sepharose was added and the preparation was incubated for 5 h at 4°C. Then the beads were washed with PBS-T three times. After washing, bead-bound proteins were eluted by boiling the preparations in 40 μl of 2× sodium dodecyl sulfate (SDS)-polyacrylamide gel electrophoresis (PAGE) sample buffer (0.125 M Tris-HCl [pH 6.8], 4% SDS, 20% glycerol, 10% mercaptoethanol). The samples were then fractionated on a 12.5% SDS-polyacrylamide gel and transferred to a polyvinylidene difluoride membrane. The membrane was then blocked for 30 min at room temperature by incubating it in PBS containing 5% skim milk. Then the membrane was probed with anti-MDP1 MAb 3A or anit-Ag85 antibodies overnight at 4°C. After probing, the membrane was washed four times with PBS-T. Next, the membrane was incubated for 4 h at room temperature with peroxidase-conjugated anti-mouse IgG or anti-rabbit IgG (Dakopatts A/S, Denmark) diluted 1:10,000. The membrane was then washed as described above, and immunoreactive bands were visualized by using an ECL Western blot detection reagent (Amersham Bioscience, Buckinghamshire, United Kingdom) according to the manufacturer's instructions.

Bead-bound glycolipids were eluted with chloroform-methanol (3:1, vol/vol). Thirty microliters of the chloroform layer was spotted on a TLC plate (HPTLC plate; 10 by 10 cm; Silica Gel 60; Merck, Darmstadt, Germany) and developed with the chloroform-methanol-acetone-acetic acid (80:20:6:1, vol/vol/vol/vol) solvent system. The TLC plate was exposed overnight to an immunoprecipitation plate (BAS-MS2025 or BAS-SR2025; Fujifilm, Japan) and visualized with the BAS system (BAS-5000). The radioactivity of separated spots was quantified by using the BAS system's software.

Analysis of mycolyltransferase activity. The mycolyltransferase catalytic reaction was analyzed by using the method developed by Belisle et al. (4). Twenty-five micrograms of TMM purified from *M. tuberculosis* H37Rv was immobilized in each glass vial, and then PBS containing 4 μl of a 1-mg/ml dithiothreitol solution and 0.5 μCi of [^{14}C]trehalose (American Radiolabeled Chemicals Inc.) were added. Two hundred micrograms of culture filtrate or 20 μg of Ag85 complex protein and various amounts of MDP1 or BSA were mixed to obtain a total

volume of 200 μl and incubated for 30 min at 37°C. Glycolipids were eluted with chloroform-methanol (2:1, vol/vol), 10 μl of the chloroform layer was spotted on a TLC plate (HPTLC plate; 10 by 10 cm; Silica Gel 60; Merck, Darmstadt, Germany), and the plate was developed with the chloroform-methanol-acetone-acetic acid (80:20:6:1, vol/vol/vol/vol) solvent system. TLC plates were analyzed by using the BAS system described above.

Construction of HLP/MDP1 complemented strain. Based on the *mdp1/hlp* nucleotide sequences, two oligonucleotide primers, forward primer 5'-GGGAA GCTTATTCGCCGCCCACCTAGT-3' and reverse primer 5'-TAACGCACCA ACGCGAAA-3', were purchased from Sigma Genosys. A PCR was carried out by targeting 10 ng chromosomal DNA of *M. smegmatis* MC^2155 with an automated thermal sequencer (Perkin Elmer). The samples were first denatured by heating them at 94°C for 5 min; then they were subjected to 30 cycles of 94°C for 1 min, 58°C for 1 min, and 72°C for 3 min and were finally incubated for 5 min at 72°C. An amplified 0.9-kb DNA fragment, which contained the promoter and structural gene of HLP/MDP1, was cloned into pGEM-T (Promega) utilizing a ligation kit (version 1, Takara), sequenced, excised by digestion with HindIII and NotI, and ligated to the same site of pMV306-Hyg, a one-copy integrated vector for the phage attachment site. pMV306-Hyg was provided by H. I. Boshoff (National Institutes of Health, Bethesda, MD). The resulting plasmid was introduced into an *M. smegmatis* HLP/MDP1 KO strain by a standard electroporation procedure (17, 39), and then a hygromycin-resistant colony was selected. Complementation was confirmed by protein expression with Western blotting using anti-MDP1 MAb 3A (data not shown).

SEM analysis. Five-milliliter portions of culture aliquots were concentrated by centrifugation (3,000 × *g*) before suspension in fresh Middlebrook 7H9-ADC medium. The OD_{600} was adjusted to 0.1, and then the preparations were placed on poly-L-lysine-coated Thermanox coverslips in 24-well tissue culture plates. The bacteria were allowed to settle for 30 min before gentle decanting and addition of 1 ml of a solution containing 2% paraformaldehyde and 2.5% glutaraldehyde in 0.1 M sodium cacodylate buffer (pH 7.4) with 0.2 M sucrose. The samples were incubated at 4°C overnight before treatment with 2% OsO_4 in 0.1 M cacodylate buffer for 2 h at room temperature. A series of sequential ethanol dehydration steps were performed (50, 70, 95, and 100% ethanol, 10 min each) before samples were dried under CO_2 using a critical point drier (HCP-2; Hitachi). Samples were Pt-Pd sputter coated (E-1030; Hitachi) and imaged with an Hitachi S-4700 scanning electron microscope (SEM). The SEM analysis was performed in triplicate using three independently grown cultures.

Chase of glycolipid synthesis. *M. smegmatis* strains, including the wild type, the MDP1 KO mutant, and the complemented strain, were precultured at 37°C in LB broth (Sigma) containing 1-mm-diameter glass beads. First, bacterial clumps were disrupted with the beads by vortexing, and then the OD_{600} was adjusted to 0.1. Then 5 μl of each bacterial suspension was added to 5 ml of fresh medium containing glass beads. [1-^{14}C]acetic acid (sodium salt; 37 MBq/ml; PerkinElmer Life & Analytical Sciences, Massachusetts) was added at a final concentration of 1 μCi/ml on day 3 or7. Each bacterial medium was incubated for 16 h and diluted to obtain 6.0 × 10^7CFU/ml. Two milliliters of this bacterial suspension was collected by centrifugation and washed with pure water three times. After the supernatants were discarded, we added 1 ml of chloroform-methanol (3:1, vol/vol) and sonicated the preparation for 30 min. Thirty microliters of the chloroform layer was spotted on a TLC plate. The radioactivity of the separated spots was quantified by using the BAS system software as described above.

MALDI-TOF mass spectrometry analysis. A matrix-assisted laser desorption ionization–time of flight (MALDI-TOF) mass spectrometry analysis was carried out by using an Ultraflex mass spectrometer (Bruker Daltonics) in the reflectron mode. Samples were dissolved in chloroform-methanol (2: 1, vol/vol) at a concentration of 1 mg/ml and applied to the sample plate as droplets. 2,5-Dihydroxybenzoic acid was used as the matrix. The accelerating voltage was 20 kV.

Construction of BCG-Luc and assessment of its growth. Linker DNAs including the Shine-Dalgarno sequence (AGCTTAGTACTGGATCCGAGGACC TGCC and GATCGGCAGGTCCTCGGATCCAGTACTA) were synthesized by Sigma Genosys. pGEM-Luc (Promega) was digested with both BamHI and HindIII, and annealed linker DNA was inserted by ligation utilizing a ligation kit (version 1; Takara). The construct was then digested with HindIII and StuI, and the gene fragment containing the Shine-Dalgarno sequence and the luciferase gene was inserted into pSO246 (25), which had been digested with BamHI, blunt ended with T4 DNA polymerase, and digested with HindIII. The resulting plasmid was designated pSO-Luc. pMV261 (39) was digested with KpnI and HindIII, and the Hsp60 promoter region was inserted into the same site of pSO-Luc. The final construct was introduced into BCG by electroporation by the method described previously (25), and the kanamycin-resistant BCG-Luc strain was obtained. BCG-Luc was grown at 37°C in Middlebrook 7H9-ADC medium until mid-log phase and collected by centrifugation. Bacteria were suspended in RPMI 1640 (Sigma) containing 10% FBS with or without MDP1 or Ag85 complex proteins in a 96-well tissue culture plate (Becton Dickinson) and incubated at 37°C. Luciferase activity was determined at each time point as described previously (12).

Statistical analyses. Data were analyzed by using a Power Macintosh G5 and StatView 5.0 (SAS Institute Inc.) and were expressed as means ± standard deviations. Data that appeared to be statistically significantly different were compared by using an analysis of variance for comparing the means of multiple groups and were considered significantly different if the *P* value was less than 0.05.

RESULTS

MDP1 binds externally to the cell wall of BCG. MDP1 acts as an adhesin on the envelope through interaction with glycosaminoglycans on the host cell surface (1, 38). Because MDP1 is retained in the cell wall, we hypothesized that MDP1 is tightly bound to some unknown targets in the cell wall. In order to assess this possibility, first we examined the binding of MDP1 to the cell wall. We incubated FLUOS-labeled MDP1 with BCG and investigated the interaction by fluorescence microscopy. The results revealed that MDP1 (pI 12.4; molecular mass, 21 kDa) bound to the surface of BCG (Fig. 1A). In contrast, other FLUOS-labeled basic proteins, such as egg white lysozyme (pI 9.2; molecular mass, 16 kDa) (Fig. 1B) and bovine histone H1 (pI 11.5; molecular mass, 21 kDa) (Fig. 1C), did not interact with BCG. Bovine serum albumin (pI 5.4) did not interact either (data not shown). Thus, MDP1 can specifically bind externally to the cell wall.

MDP1 binds to TMM and TDM but not to free mycolic acids. Mycolic acids form an ordered structure in the envelope and are believed to be some of the outermost covalently linked elements (3, 20). *M. tuberculosis* produces three kinds of mycolic acids, the alpha-, methoxy-, and keto-mycolates. Three types of MAMEs (alpha-, methoxy-, and keto-mycolates), as well as TMM and TDM derived from *M. tuberculosis* strain Aoyama B, were immobilized on an ELISA plate and reacted with MDP1, and the interaction was detected with anti-MDP1 MAb 3A (subclass IgG1, light chain κ). The affinity of MAb 3A for MDP1 was 1.39 e^{-9} M as determined by surface plasmon resonance analysis with a Biacore biosensor (Biacore) (data not shown). This MAb binds to neither TMM nor TDM (data not shown). The results showed that MDP1 bound to TMM and TDM but not to any type of MAME (Fig. 1D). This indicates that MDP1 specifically recognizes the covalent linkage of mycolic acids to the 6-hydroxyl group of trehalose, because MDP1 does not bind to any mycolic acid (Fig. 1D) or free trehalose (1).

Physiological interaction between MDP1 and glycolipid in the mycobacterial cell wall. Next we examined whether MDP1 actually associated with TMM and TDM in the mycobacterial envelope by using an immunoprecipitation assay. A cell wall fraction derived from BCG by the method described previously (27) was incubated with MAb 3A or control mouse IgG. Then MDP1-bound glycolipids were precipitated with protein G-coupled beads, extracted with an organic solvent (chloroform-methanol, 3:1 [vol/vol]), and analyzed by TLC. Both TMM and TDM were precipitated by MAb 3A but not by control IgG (Fig. 1E), showing that MDP1 associated with TDM and TMM in the cell wall. The data also showed that MDP1 bound to other unknown lipids that migrated above TDM, as well as below TMM (Fig. 1E).

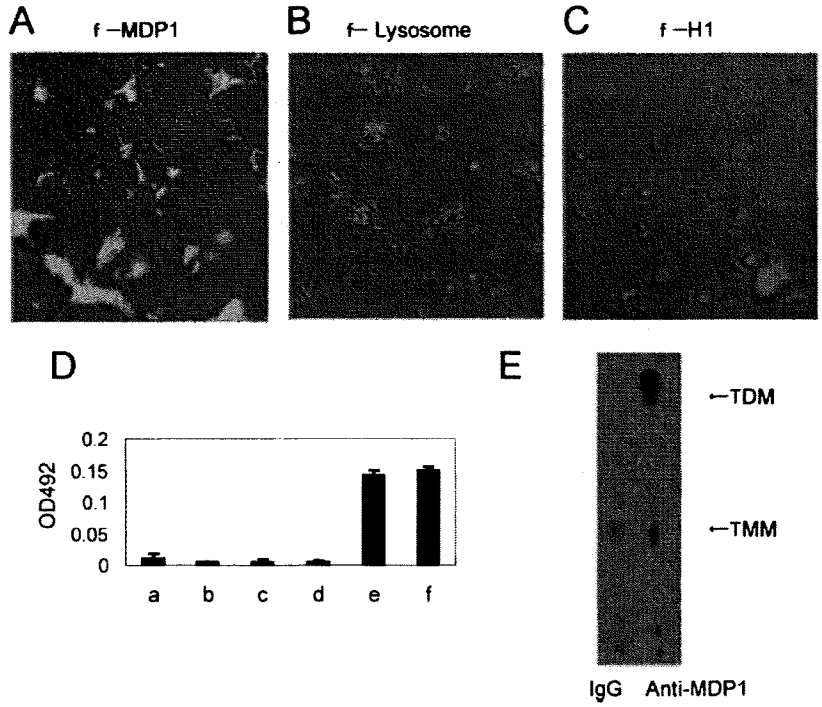

FIG. 1. MDP1 binds to the cell wall of BCG. (A to C) BCG was incubated with FLUOS-labeled MDP1 (A), egg white lysozyme (B), and bovine histone H1 (C). Bacteria were viewed with a confocal scanning laser microscope. (D) ELISA to detect MDP1-lipid or -glycolipid interactions. Mycolic acids (bar b, alpha-MAME; bar c, methoxy-MAME; bar d, keto-MAME) and glycolipids (bar e, TMM; bar f, TDM) were immobilized on an ELISA plate and reacted with MDP1, and the level of binding was detected with anti-MDP1 MAb 3A. Bar a shows the results for a negative control without immobilization of either lipids or glycolipids. OD492, optical density at 492 nm. (E) Immunoprecipitation assay to detect physiological interaction of MDP1 and glycolipid. Cell wall derived from BCG was incubated with anti-MDP1 MAb 3A or control mouse IgG in the presence of protein G-coated Sepharose. Samples were spotted on a TLC plate and developed with the chloroform-methanol-acetone-acetic acid (80:20:6:1, vol/vol/vol/vol) solvent system.

MDP1 regulates transfer of mycolic acids by Ag85 complex proteins in vitro. We next examined the effect of MDP1 on transfer of mycolic acids by Ag85 complex proteins, because MDP1 can bind TMM and TDM, which are substrates of Ag85 complex proteins. We purified Ag85 complex proteins, as well as Ag85A, Ag85B, and Ag85C individually, from *M. tuberculosis* H37Rv by the method described previously (28). Purified Ag85 complex proteins transferred mycolic acids to ^{14}C-labeled trehalose as described previously (4). A molar amount of MDP1 equivalent to that of the Ag85 complex reduced synthesis of TDM and TMM by 44.4% ± 18.4% and 57.4% ± 25.2%, respectively (Fig. 2A and 2B). In contrast, a molar ratio of MDP1 to Ag85 proteins of 1/1,000 enhanced synthesis of TDM and TMM by 36.8% ± 32.4% and 36.4% ± 22.1%, respectively (Fig. 2A and 2B). The same results were obtained when total culture filtrates were used (Fig. 2C, upper chromatogram) or when purified Ag85B was used (Fig. 2C, lower chromatogram). These results demonstrate that MDP1 possesses an activity to control the function of mycolyltransferases.

MDP1 binds to Ag85 complex proteins. Because MDP1 controlled transfer of mycolic acids in the presence of excess amounts of substrate (TMM) (Fig. 2), we considered the possibility that MDP1 interacts not only with TMM but also with Ag85 complex proteins, which we examined next. Ag85A, Ag85B, or Ag85C was immobilized on ELISA plates by serial concentration and then incubated with MDP1. The level of binding of MDP1 to Ag85 complex proteins was detected by anti-MDP1 MAb. The results showed that the interaction between MDP1 and each Ag85 complex protein produced standard binding curves (Fig. 3A). BSA did not bind to MDP1. These results suggested that MDP1 binds to all Ag85 proteins.

Ag85 complex proteins bind to fibronectin by the motif conserved in the complex, which is comprised of 11 amino acid residues (29). We examined if this region also participated in the MDP1-Ag85 complex protein interaction. However, neither human fibronectin nor synthetic peptide corresponding to the region from position 98 to position 108 of Ag85B, which inhibits an Ag85 complex-fibronectin interaction, inhibited an MDP1-Ag85 complex protein interaction (data not shown). Thus, Ag85 complex proteins associate with MDP1 through a region other than the fibronectin-binding site.

We next examined whether MDP1 interacted with Ag85 complex proteins in the mycobacterial cell wall. A cell wall fraction derived from BCG was immunoprecipitated with MAb 3A or control mouse IgG and separated by SDS-PAGE. One gel was stained with Coomassie brilliant blue R250, and another gel was used for Western blot analysis. Although we observed only faint bands corresponding to Ag85 complex proteins (Ag85A and Ag85C at 32 kDa and Ag85B at 30 kDa) in the stained gel, in the Western blot analysis we observed that the bands reacted with anti-Ag85 complex protein Ig in the

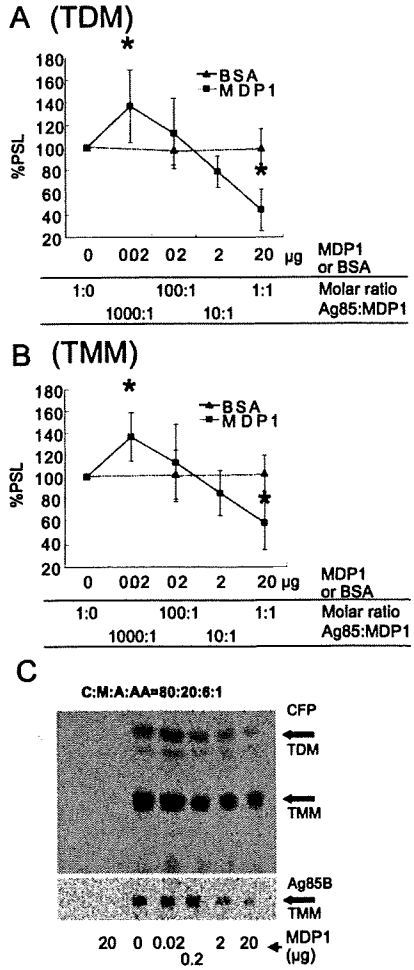

FIG. 2. MDP1 regulates mycolyltransferase activity in vitro. (A and B) Radioactivity of ^{14}C-labeled TDM (A) and TMM (B) synthesized by Ag85 complex proteins in vitro was quantified by using the BAS system software. Radioactivity was expressed as a percentage of the value for the sample without MDP1, which was defined as 100%. Similar experiments were performed utilizing BSA instead of MDP1, and the results were compared. PSL, photo-stimulated luminescence. Asterisk, $P < 0.05$ for a comparison with control BSA (0 or 20 μg) (as determined by analysis of variance). (C) Culture filtrate (CFP) (upper chromatogram) or Ag85B (lower chromatogram) was added to each vial and incubated for 30 min at 37°C in the presence of various doses of MDP1 and [^{14}C]trehalose, and then glycolipids were eluted with chloroform-methanol (2:1, vol/vol). Biosynthesis of glycolipids was analyzed by using the BAS system after TLC plates were developed with the chloroform-methanol-acetone-acetic acid (C:M:A:AA) (80:20:6:1, vol/vol/vol/vol) solvent system. The lane on the left contained a negative control without culture filtrate and Ag85B.

precipitates when anti-MDP1 MAb was used but not when control IgG was used (Fig. 3B). Similar experiments were performed with anti-Ag85 Ig. Anti-Ag85 Ig, but not control Ig, precipitated MDP1 from the cell wall fraction of BCG (Fig. 3C). Taken together, these results suggest that the Ag85 complex proteins associate with MDP1 in the cell wall.

Subcellular localization of MDP1 in the course of culture. We analyzed the MDP1 content of the cell wall during the course of culture. We cultured *M. smegmatis* in LB medium for

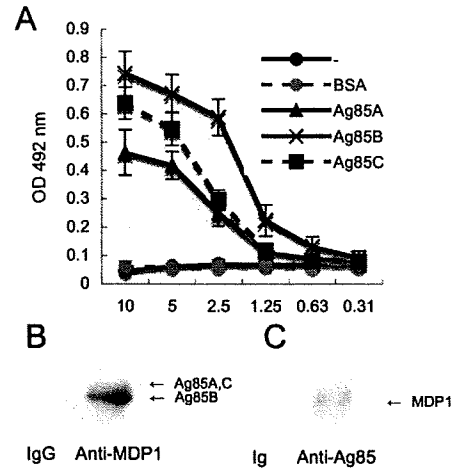

FIG. 3. MDP1 binds to Ag85 complex proteins. (A) ELISA to detect the MDP1-Ag85 complex protein interaction. BSA, Ag85A, Ag85B, and Ag85C were immobilized on an ELISA plate by incubating various concentrations of proteins and reacted with MDP1, and the binding was detected with anti-MDP1 MAb. −, results without immobilized proteins. OD 492 nm, optical density at 492 nm. (B and C) Immunoprecipitation assay to detect a physiological interaction between MDP1 and Ag85 complex proteins. Cell walls derived from BCG were incubated with (B) anti-MDP1 MAb 3A (Anti-MDP1) or control mouse IgG (IgG) or (C) with anti-Ag85 Ig (Anti-Ag85) or control rabbit Ig (Ig) in the presence of protein G-coated Sepharose. Samples for Western blotting were probed with rabbit anti-Ag85 Ig (B) or anti-MDP1 MAb (C).

3, 5, and 7 days, and each subcellular fraction was purified. In this experiment, bacteria grew to stationary phase by day 4 (Fig. 4A). The MDP1 content in each fraction was analyzed by Western blotting. The results showed that MDP1 accumulated in both cell wall and other cellular fractions (membrane, ribosome, and cytoplasmic fractions) at the stationary growth phase (Fig. 5A).

We next carried out a similar experiment with BCG. Total cellular proteins, the cell wall fraction, and other cellular fractions were obtained from BCG after growth for 10, 20, 30, and 60 days on Sauton medium. A Western blot analysis showed that the cellular content of MDP1 increased in both the cell wall and other cellular fractions (Fig. 5B), while the levels of Ag85 complex proteins in the cell wall decreased with time (Fig. 5C).

Role of MDP1 in glycolipid biosynthesis. MDP1 is presumed to be essential in slow growers, such as *M. tuberculosis* (34). However, the *mdp1/hlp* gene can be knocked out in *M. smegmatis* (19). In order to determine the physiological role of MDP1 in assembly of the cell wall, we employed an *M. smegmatis* MDP1/HLP KO strain constructed by the group of Thomas Dick (19). We additionally generated an MDP1-complemented strain by insertion of a single copy of the *M. smegmatis* MDP1 gene into the genome of the MDP1/HLP KO strain.

We first analyzed the growth kinetics of the wild type, the MDP1 KO strain, and the complemented strain in LB medium. In this experiment, all strains reached stationary phase on day 4, but the bacterial density of the MDP1 KO strain was lower than that of the wild-type strain during the stationary growth

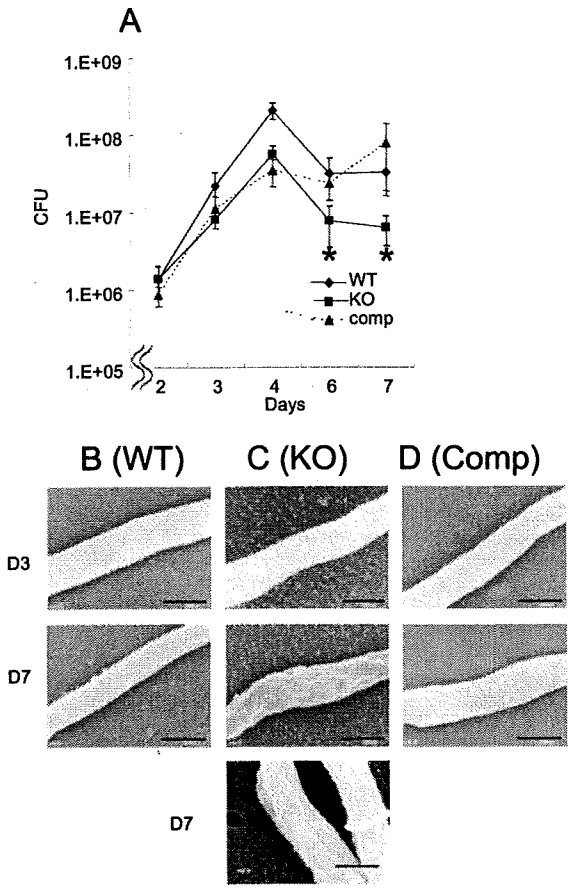

FIG. 4. Effect of MDP1 deficiency on growth kinetics and cell surface morphology. (A) Wild-type *M. smegmatis* mc^{2}155, MDP1 KO, and complemented strains were cultured in LB broth, and bacterial numbers at various time points were determined and expressed as CFU after serially diluted samples on LB agar were harvested. Asterisk, $P < 0.05$ for a comparison with the wild-type strain (as determined by analysis of variance). The results are the results of one representative experiment of seven experiments in which similar results were obtained. (B to D) Visualization of cell surface structure of the wild-type (WT) (B), MDP1 KO (KO) (C), and complemented (Comp) (D) strains by SEM. Bars = 0.5 μm. Bacteria in both exponential (day 3 [D3]) and stationary (day 7 [D7]) phases were analyzed.

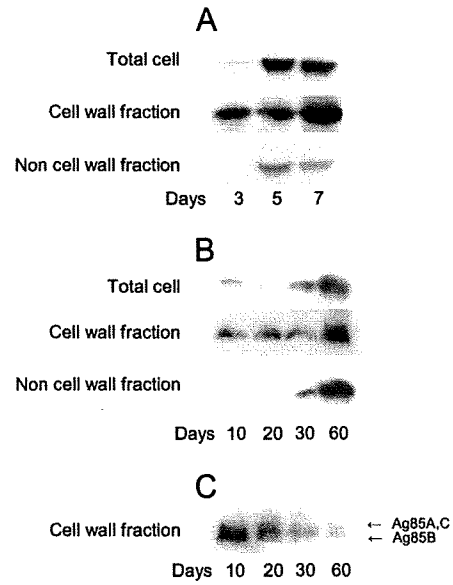

FIG. 5. Subcellular localization of MDP1 and Ag85 in the course of culture. (A to C) Total cellular protein (Total cell), the cell wall fraction (Cell wall fraction), and the residual material after isolation of the cell wall fraction (Non cell wall fraction) were obtained from *M. smegmatis* (A) and BCG (B and C) at each time point indicated. The samples were analyzed by Western blotting with anti-MDP1 MAb 3A (A and B) or anti-Ag85B Ig (C). The data are representative of three to five experiments.

phase (Fig. 4A). This phenotype was almost completely reversed by complementation. Next, we analyzed bacterial surface morphology by SEM. All strains produced similar smooth structures at exponential phase (Fig. 4B, C, and D, upper panels), and both the wild-type and complemented strains were normal with a smooth shape even in the stationary growth phase (Fig. 4B and D, middle panels). However, at the same time point, the MDP1 KO strain displayed a crenellated structure (Fig. 4C, middle and lower panels), implying that MDP1 influences cell envelope structure during stationary phase in *M. smegmatis*.

In order to analyze the effect of MDP1 disruption on glycolipid biosynthesis, we chased synthesis of mycolates and TMM by adding ^{14}C-labeled acetic acid to cultures of the wild-type, MDP1 KO, and complemented strains. Incorporation of radioactivity into TMM and MAMEs was analyzed by using the BAS system after fractionation by high-performance TLC (Fig. 6). TLC analysis revealed two TMM spots (Fig. 6A). *M. smegmatis* produces three types of mycolic acids, alpha, alpha′, and epoxy mycolates. To determine which types of mycolates were present in each TMM spot, we determined the molecular mass of each spot by MALDI-TOF mass spectrometry. The major peak of the upper TMM spot showed a pseudomolecular ion $[M+Na]^+$ at *m/z* 1556, which was identified as alpha-C_{83} TMM, while the major peak of the lower spot showed a pseudomolecular ion $[M+Na]^+$ at *m/z* 1306, which was presumed to be alpha′-C_{65} TMM (data not shown) (14). Thus, high-performance TLC analysis can separate alpha TMM and alpha′ TMM.

The three strains synthesized similar amounts of TMM and MAMEs during exponential growth (day 3). However, during stationary phase (day 7), in both the wild-type and complemented strains mycolate synthesis was reduced strongly (day 7). By contrast, the MDP1-deficent strain continued production of both mycolates and TMM, synthesizing 9.9-fold-higher amounts of TMM (Fig. 6B), 4.3-fold-higher amounts of alpha-MAME (Fig. 6C), and 5.9-fold-higher amounts of alpha′-MAME (Fig. 6D) than the wild type. This phenotype was completely reversed by complementation, indicating that a lack of MDP1 impaired the down-regulation of biosynthesis of mycolates and TMM in stationary phase.

Altering the growth rate with Ag85 complex proteins and MDP1. Because cell wall biogenesis is a biological event involved in multiplication of bacteria, we next examined whether regulation of the transfer of mycolic acids by MDP1 influences mycobacterial growth. We assessed the effects of exogenously

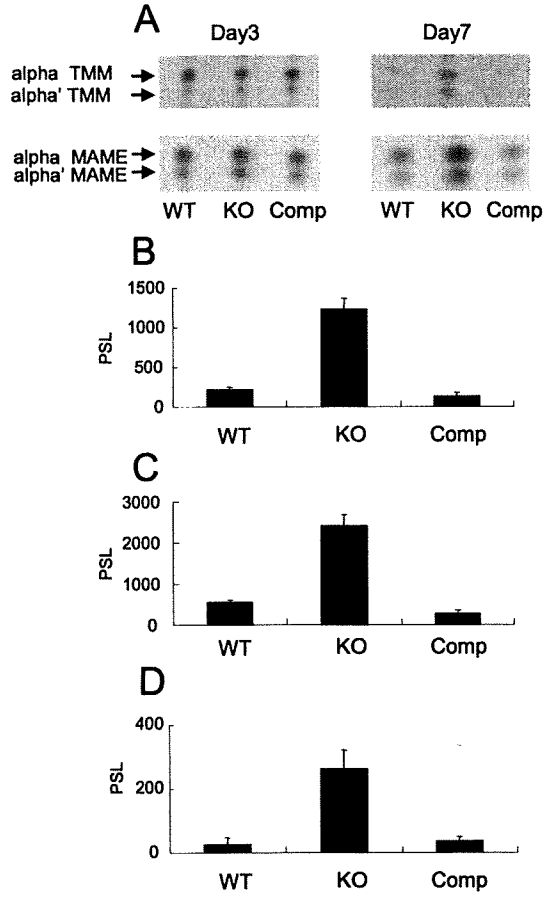

FIG. 6. MDP1 mediates cessation of glycolipid biosynthesis at the stationary growth phase. (A) Lipid synthesis was measured by addition of [^{14}C]acetate to a bacterial culture. The TMM and MAMEs from 10^8 bacteria, including the *M. smegmatis* parent strain (wild type [WT]), the MDP1 KO strain (KO), and the complemented strain (Comp), were extracted on days 3 and 7 and fractionated by TLC. The radioactivities of synthesized TMM and MAMEs were visualized by using the BAS system. (B to D) Radioactivities of TMM (B), alpha-MAME (C), and alpha'-MAME (D) extracted from a bacterial culture after 7 days were quantified by using the BAS system software and compared for the wild-type, MDP1 KO, and complemented strains. The values are means ± standard deviations of five experiments. PSL, photostimulated luminescence.

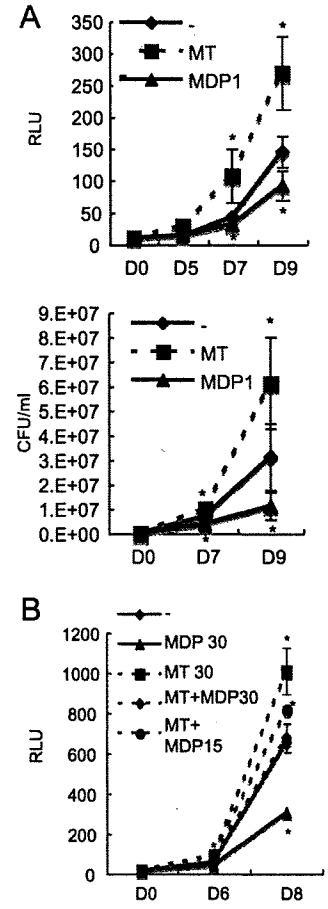

FIG. 7. Growth control of BCG by exogenously added MDP1 and Ag85 complex proteins. BCG-Luc was grown in RPMI 1640 containing 10% FBS in the presence of various doses of MDP1, Ag85 complex, or a mixture of MDP1 and the Ag85 complex in a 96-well tissue culture plate. The total culture volume was 200 μl in each well. Representative results of three independent experiments are presented. (A) Luciferase activity (expressed in relative luciferase units [RLU]) was measured on days 0, 5, 7, and 9 (upper graph), and CFU were counted on days 0, 7, and 9 (lower graph). MT, 30 μg/well Ag85 complex; MDP1, 30 μg/well MDP1; −, BCG-Luc alone. The values are the means ± standard deviations of three experiments. (B) Luciferase activity was measured on days 0, 6, and 8. MT 30, 30 μg/well Ag85 complex; MDP 30, 30 μg/well MDP1; MT+MDP30, 30 μg/well Ag85 complex plus 30 μg/well MDP1; MT+MDP15, 30 μg/well Ag85 complex plus 15 μg/well MDP1; −, BCG-Luc alone. The values are the means ± standard deviations of three experiments. Asterisk, $P < 0.05$ for a comparison with the no-protein control (as determined by analysis of variance).

added MDP1 in culture media on this growth. We generated a luciferase-producing BCG strain (BCG-Luc) to estimate the growth of BCG. The activity of luciferase paralleled the CFU assay results up to 10^4 CFU/ml (data not shown). We cultured BCG-Luc in the presence or absence of MDP1 or Ag85 complex proteins. Both the luciferase-based assay and determination of the CFU showed that exogenously added MDP1 suppressed growth of BCG, while Ag85 complex proteins enhanced growth (Fig. 7A). We next added serial doses of MDP1 to the culture of BCG-Luc in the presence of Ag85 complex proteins. We found that a low dose of MDP1 further boosted Ag85 complex-induced growth enhancement, while a high dose of MDP1 suppressed Ag85-dependent growth enhancement (Fig. 7B).

DISCUSSION

In this study, we analyzed the role of the mycobacterial histone-like protein MDP1 in the cell wall. We found that MDP1 plays an important role in tuning cell wall assembly by controlling transfer of mycolic acids to sugars by Ag85 complex proteins.

We showed that the cellular content of MDP1 was increased in advanced cultures of both *M. smegmatis* and BCG (Fig. 5). Previously, we and other groups showed that MDP1/HLP was accumulated in growth-retarded phases, including dormant bacilli of *M. tuberculosis* and *M. smegmatis* (19, 26, 37), by one-

dimensional SDS-PAGE analysis. MDP1 is resistant to analysis by two-dimensional gel electrophoresis because of its strong positive charge (pI of BCG, 12.4; pI of *M. tuberculosis*, 12.45). However, in spite of the extensive analysis of gene expression profiles with DNA microarrays, increased expression of *mdp1* mRNA in a stationary or anaerobic culture has not been observed (5, 18, 30, 35, 42). These results imply that accumulation of MDP1 in growth-retarded phases is largely due to posttranscriptional regulation. Pethe et al. found that lysines of the C-terminal region of laminin-binding protein/MDP1 are methylated by an unknown enzyme, which is present at a high level in the cell wall and confers resistance to proteolysis (31). Thus, posttranslational modification stabilizes MDP1 and might be involved in accumulation of MDP1 during a growth-retarded phase. In addition, methylation of basic charged amino acids may help the association of MDP1 with glycolipids by negating the charge of the protein. Posttranslational modifications, resembling eukaryotic histones, may control the cellular function and stability of MDP1. This issue should be clarified by additional study. By contrast, Ag85 complex proteins were localized in the cell wall during culture, but the contents gradually decreased with time in BCG (Fig. 5C) and *M. smegmatis* cultures (data not shown). It is likely that mycobacteria regulate transfer of mycolic acids by altering amounts of both MDP1 and Ag85 complex proteins in the cell wall.

The density of the MDP1 KO strain was lower in stationary phase (Fig. 4A). Lee et al. reported that an HLP/MDP1 KO strain displayed the same growth kinetics in Dubos Tween-albumin broth (19). We confirmed that an *M. smegmatis* MDP1 KO strain exhibited similar levels of cell density and survival at stationary phase when it was cultured in Dubos Tween-albumin broth (data not shown). Furthermore, alteration of the surface structure at stationary phase was not revealed by SEM analysis of the surface of the MDP1 KO strain cultured in Dubos Tween-albumin broth (data not shown).

TMM-derived mycolic acids are a major source of TDM and AG-linked mycolic acids (40, 41). Thus, the amount of TMM is an important factor for determining the level of cell wall assembly. The MDP1 KO strain exhibited continued synthesis of TMM other than MAMEs (Fig. 6) and TDM (data not shown) at the stationary growth phase. TMM could be synthesized from TMM and TDM by Ag85 complex proteins, once the substrates (TMM and TDM) were synthesized. However, the primary enzyme that catalyzes synthesis of TMM is still not known. Takayama et al. proposed that TMM could be synthesized in the cytoplasm (40). However, recently, Tropis et al. demonstrated that TMM is synthesized outside the plasma membrane but not inside the cytoplasm (41). The Ag85 complex is the most abundant protein secreted by *M. tuberculosis* (around 10 to 30%) and is a possible candidate enzyme for transfer of mycolic acids to trehalose to synthesize the TMM precursor (β-keto-acyl trehalose), as deduced from the structure of Ag85C (33). MDP1 suppresses Ag85 complex-dependent secondary synthesis of TMM (Fig. 2B), but we cannot eliminate the possibility that MDP1 also inhibits the primary synthesis of the TMM precursor whenever it is catalyzed by Ag85 complex proteins or undetermined enzymes.

An activity controlling glycolipid biosynthesis prompted us to examine whether exogenously added MDP1 and Ag85 complex proteins influence bacterial growth. We showed that growth of BCG could be altered by a combination of Ag85 complex proteins and MDP1 (Fig. 7). The MDP1 content in the total proteins of the cell wall increased at the stationary growth phase, while that of the Ag85 complex proteins decreased (Fig. 3). It can be speculated that a change in the ratio of MDP1 to Ag85 complex proteins in the cell wall is involved in determining the growth rate.

Inhibition of specific cellular metabolism causes cell death, as many antibiotics kill bacteria. However, expression of MDP1 does not kill mycobacteria; instead, it just suppresses growth (23). This is probably due to suppression of whole cellular metabolism, including macromolecular biosynthesis of DNA, RNA, and proteins (23) and cell wall assembly, as shown in this study. This can be caused by multiple interacting activities of different classes of macromolecules. The mechanism of such multiple binding activities should be resolved by structure-based studies, like those done on bacterial proteins such as SecB (32, 44). Recently, it has been reported that the histone-like protein HN-S mediates silencing of global gene expression in growth-retarded *Salmonella* (2, 8, 21). In humans, histone H2A seems to be involved in X chromosome inactivation (11). It can be speculated that use of a nonspecific DNA-binding protein to inactivate cellular metabolism is a general strategy. Here we found an alternative role of a histone-like protein in bacterial metabolism. Our data suggest that MDP1-medaited control of glycolipid biosynthesis is involved in the mechanism linking the growth state and cell wall biogenesis. Although we conducted experiments using nonpathogenic or slightly pathogenic mycobacteria, such as *M. smegmatis* and BCG, these bacteria share the basic structure of the cell wall with pathogenic mycobacteria, including *M. tuberculosis*. Taken together, our data provide significant information for understanding both the coordination of bacterial growth and virulence.

ACKNOWLEDGMENTS

We are grateful to Keizou Oka, Department of Bioscience, INCS, Ehime University, for technical assistance with preparation of MAbs and to Thomas Dick, Novartis Institute for Tropical Diseases, for providing the *M. smegmatis* HLP/MDP1 KO strain. We also thank Todd P. Primm and Charles Scanga for editing the manuscript and Sara Matsumoto for heartfelt encouragement.

This work was supported by grants from the Ministry of Health, Labor and Welfare (Research on Emerging and Re-emerging Infectious Diseases, Health Sciences Research Grants), The Japan Health Sciences Foundation, the Ministry of Education, Culture, Sports, Science and Technology, and The United States-Japan Cooperative Medical Science Program against Tuberculosis and Leprosy.

We have no competing interests.

REFERENCES

1. **Aoki, K., S. Matsumoto, Y. Hirayama, T. Wada, Y. Ozeki, M. Niki, P. Domenech, K. Umemori, S. Yamamoto, A. Mineda, M. Matsumoto, and K. Kobayashi.** 2004. Extracellular mycobacterial DNA-binding protein 1 participates in *Mycobacterium*-lung epithelial cell interaction through hyaluronic acid. J. Biol. Chem. **279**:39798–39806.
2. **Asakura, H., K. Kawamoto, T. Shirahata, and S. Makino.** 2004. Changes in *Salmonella enterica* serovar Oranienburg viability caused by NaCl-induced osmotic stress is related to DNA relaxation by the H-NS protein during host infection. Microb. Pathog. **36**:147–151.
3. **Barry, C. E., III, R. E. Lee, K. Mdluli, A. E. Sampson, B. G. Schroeder, R. A. Slayden, and Y. Yuan.** 1998. Mycolic acids: structure, biosynthesis and physiological functions. Prog. Lipid Res. **37**:143–179.
4. **Belisle, J. T., V. D. Vissa, T. Sievert, K. Takayama, P. J. Brennan, and G. S. Besra.** 1997. Role of the major antigen of *Mycobacterium tuberculosis* in cell wall biogenesis. Science **276**:1420–1422.